

ACCEPTED MANUSCRIPT

High-power gyrotrons for electron cyclotron heating and current drive

To cite this article before publication: Manfred Thumm *et al* 2019 *Nucl. Fusion* in press <https://doi.org/10.1088/1741-4326/ab2005>

Manuscript version: Accepted Manuscript

Accepted Manuscript is “the version of the article accepted for publication including all changes made as a result of the peer review process, and which may also include the addition to the article by IOP Publishing of a header, an article ID, a cover sheet and/or an ‘Accepted Manuscript’ watermark, but excluding any other editing, typesetting or other changes made by IOP Publishing and/or its licensors”

This Accepted Manuscript is © **EURATOM 2019**.

During the embargo period (the 12 month period from the publication of the Version of Record of this article), the Accepted Manuscript is fully protected by copyright and cannot be reused or reposted elsewhere. As the Version of Record of this article is going to be / has been published on a subscription basis, this Accepted Manuscript is available for reuse under a CC BY-NC-ND 3.0 licence after the 12 month embargo period.

After the embargo period, everyone is permitted to use copy and redistribute this article for non-commercial purposes only, provided that they adhere to all the terms of the licence <https://creativecommons.org/licenses/by-nc-nd/3.0>

Although reasonable endeavours have been taken to obtain all necessary permissions from third parties to include their copyrighted content within this article, their full citation and copyright line may not be present in this Accepted Manuscript version. Before using any content from this article, please refer to the Version of Record on IOPscience once published for full citation and copyright details, as permissions will likely be required. All third party content is fully copyright protected, unless specifically stated otherwise in the figure caption in the Version of Record.

View the [article online](#) for updates and enhancements.

High-Power Gyrotrons for Electron Cyclotron Heating and Current Drive

M K A Thumm¹, G G Denisov², K Sakamoto³ and M Q Tran⁴

¹ Karlsruhe Institute of Technology (KIT), IHM and IHE, D-76131 Karlsruhe, Germany

² Institute of Applied Physics (IAP) of the Russian Academy of Sciences (RAS), Nizhny Novgorod 603950, Russia

³ National Institutes for Quantum and Radiological Science and Technology (QST), Naka, Ibaraki, 311-0193, Japan

⁴ Swiss Plasma Center (SPC), Ecole Polytechnique Fédérale de Lausanne (EPFL), CH-1015 Lausanne, Switzerland

E-mail: manfred.thumm@kit.edu

Abstract: In many tokamak and stellarator experiments around the globe that are investigating energy production via controlled thermonuclear fusion, electron cyclotron heating and current drive (ECH&CD) are used for plasma start-up, heating, non-inductive current drive and MHD stability control. ECH will be the first auxiliary heating method used on ITER. Megawatt-class, continuous wave (CW) gyrotrons are employed as high-power millimeter (mm)-wave sources. The present review reports on the worldwide state-of-the-art of high-power gyrotrons. Their successful development during the past years changed ECH from a minor to a major heating method. After a general introduction of the various functions of ECH&CD in fusion physics, especially for ITER, Section 2 will explain the fast-wave gyrotron interaction principle. Section 3 discusses innovations on the components of modern long-pulse fusion gyrotrons (magnetron injection electron gun (MIG), beam tunnel, cavity, quasi-optical output coupler, synthetic diamond output window, single-stage depressed collector) and auxiliary components (superconducting magnets, gyrotron diagnostics, high-power calorimetric dummy loads). Section 4 deals with present megawatt-class gyrotrons for ITER, W7-X, LHD, EAST, KSTAR and JT-60SA, and also includes tubes for moderate pulse length machines as, ASDEX-U, DIII-D, HL-2A, TCV, QUEST and GAMMA-10. In Section 5 the development of future advanced fusion gyrotrons is discussed. These are tubes with higher frequencies for DEMO, multi-frequency (multi-purpose) gyrotrons, stepwise frequency tunable tubes for plasma stabilization, injection-locked and coaxial-cavity multi-megawatt gyrotrons, as well as sub-THz gyrotrons for collective Thomson scattering (CTS). Efficiency enhancement via multi-stage depressed collectors, fast oscillation recovery methods and reliability, availability, maintainability and inspectability (RAMI) will be discussed at the end of this section.

Keywords: Gyrotron, tokamak, stellarator, electron cyclotron heating and current drive (ECH&CD), collective Thomson scattering (CTS), ITER, DEMO

1. Introduction

It is well known that to reach thermonuclear fusion conditions, magnetically confined plasmas require external heating up to 100-200 million Kelvin [1]. While the considerations presented in [1] show the need for additional heating power, it is important to note that each specific heating method has specific features. For example, ref. [2] is a study of the heating mix for ITER: 20 MW of electron cyclotron wave heating (ECH), 20 MW of ion cyclotron wave heating (ICH) and 33 MW of 1 MeV neutral beam injection heating (NBI). References on radio frequency (RF) heating can be found for example in [3, 4, 5]. In the present section, the missions, which can be covered by ECH and non-inductive Electron Cyclotron Wave Current Drive (ECCD) are outlined.

Here the role of electron cyclotron waves (ECWs) in magnetically confined fusion plasmas is briefly summarized. ECWs are absorbed at the plasma location, where the following resonance relation is fulfilled

$$\omega = n\Omega_{co}(r) + k_{\parallel}v_{\parallel} \quad , \quad n = 1, 2, \dots \quad (1)$$

where ω and k_{\parallel} are the angular frequency and wave vector along the toroidal direction, respectively, v_{\parallel} is the toroidal electron drift velocity, $\Omega_{co}(r)$ is the local electron cyclotron frequency and n is the cyclotron harmonic number.

The local non-relativistic electron cyclotron frequency $\Omega_{co}(r)$ is given by

$$\Omega_{co}(r) = eB_T(r)/m_o \quad (2)$$

where e and m_o are the charge and rest mass, respectively, of an electron and $B_T(r)$ is the magnitude of the local toroidal magnetic field.

The relativistic version of the resonance condition (1) is given by

$$n\Omega_{co}(r)/\omega = \gamma - N_{\parallel}u_{\parallel} \quad (3)$$

where u is the normalized relativistic momentum $u = p/m_o c$, with c being the free-space velocity of light, γ is the relativistic Lorentz factor

$$\gamma = [1 + u^2]^{1/2} \quad (4)$$

and N_{\parallel} is the component of the vector refractive index $N = kc/\omega$ parallel to B_T .

When k_{\parallel} is zero (perpendicular injection), absorption occurs at the plasma location where the local cyclotron frequency ($n = 1$) or its harmonics ($n > 1$) matches the wave frequency. The term $k_{\parallel}v_{\parallel}$ denotes the Doppler shift for an obliquely launched wave.

The physics of ECH&CD, such as mode of propagation, cut-off and resonance, absorption coefficient, and current drive efficiency can be found in [1,5]. Clearly, since the toroidal magnetic field B_T in a tokamak depends on the radial location in the plasma (B_T decreases inversely with the major radius), the required frequency of the ECWs will be dependent on the desired localization of the heating or current drive region in the plasma. The relation between the non-relativistic EC frequency f_{c0} and the local toroidal magnetic field is simply f_{c0} [GHz] = $\Omega_{co}/2\pi = 28 * B_T$, when B_T is expressed in Tesla. In the case of current drive, the waves are obliquely launched and therefore there will be an upshift of the resonance frequency compared to the local f_{c0} . The value of this upshift is discussed in the paper by Poli et al. [6]. The application of formulas (3) and (4) of ref. [6] yields an upshift factor in the range of 1.2-1.4, depending on the launching angle and the plasma parameters (the local electron temperature). Therefore the CD frequency is given by f_{CD} [GHz] = (1.2-1.4)* 28* B_T . The selection of the optimum frequency for a specific CD function for a given plasma configuration (density profile, temperature profiles) and machine parameters (magnetic field, possible launching points), requires a full optimization calculation. Trade-off may be needed, taking into account the optimally determined frequency and what could be achieved technically. Often, as discussed below, an ECW system will combine both heating and current drive functions. Space and cost constraints lead to the selection of a compromise between the optimum frequency for each function. As described later, the availability of gyrotrons operating at 2 or 3 frequencies (determined by the resonant frequencies of the dielectric window at the output of the tube) or step-tunable (in step of 2-3 GHz over a bandwidth of approx. ± 10 GHz) with a broadband output window opens up new domains of flexibility in the design and implementation of ECH&CD systems.

ECWs can be used in magnetically confined plasmas for various functions from the plasma start-up to ramp down. They encompass: a) the plasma breakdown including the start of the tokamak current, b) the so-called ramp-up phase in which the current is ramped up to the nominal current and the plasma brought into the H mode, c) plasma control and MHD control during the burn phase and d) the ramp down of the plasma current. ECWs can even be used for vessel cleaning [7].

1
2
3 The necessity of using ECWs for the plasma breakdown in tokamaks arises due to the limitation of the
4 toroidal E -field during this phase to a value of around 0.3 V/m. The requirements on frequency are
5 relatively flexible. For example, in ITER, the same 170 GHz gyrotrons will be used for breakdown as
6 well as heating, current drive and control of the MHD instabilities [8].
7

8 The next phase is to bring the plasma into the H mode. The scaling law used most often (the so-called
9 "Martin scaling law") is described in [9]. For this function, heating is the main point. For large devices
10 like ITER and DEMO, the total power can be relatively high [9,10], depending on the scenarios which
11 will be adopted. For DEMO, where the required power is in the range of 150 MW, an optimization of
12 the ramp-up scenarios is still under way in view of minimizing the required power during this phase. A
13 second point to be noted is that this function can be fulfilled with other heating methods, provided that
14 the power can be absorbed by the plasma during its trajectory from low-plasma current I_P to the flat top
15 phase. In this sense, ECWs can be used at low plasma density, as noted in [10].
16

17 In subsequent phases of a fusion plasma, ECWs can fulfil various control functions, such as sawtooth
18 period control [11], neo classical tearing mode (NTM) control [12], as well the control of the H to L
19 mode transition during the ramp-down phases. In each case, the requirements for the gyrotrons (power,
20 frequency) and for the launchers at the torus must be determined based on the plasma scenarios and
21 plasma profiles. Examples of such calculations can be found in [6,13]. Optimization of the frequency
22 for the current drive function is described in [6].
23

24 Before concluding on the physics requirements from the gyrotron side, it is worth mentioning a few
25 trends, which are often driven by the users:
26

- 27
28 (a) even in present devices in operation, both tokamaks and stellarators, the power per gyrotron is
29 at the 1 MW level. This brings some cost reduction on the ancillary system (superconducting
30 gyrotron magnets) as well as on the transmission lines and launchers. For future devices such
31 as DEMO, a total required power of 50 MW [13] or more is considered: this leads to a desirable
32 gyrotron unit power of 2 MW;
- 33 (b) as already mentioned above, to fulfil the different functions required by physics, the ECW power
34 is deposited at different locations in the plasma, with different upshift (= 1 for heating, between
35 1.2-1.4 for functions linked to current drive physics). In some medium size tokamaks such as
36 TCV, the low value of B_T leads to the use of ECWs at the second harmonic or even the third
37 harmonic to allow access to high plasma density [14]. In both cases, the possibility of having
38 gyrotrons operating at two or more frequencies (determined by the transmission frequencies of
39 the output window), or which can be magnetically tuned over the different resonant frequencies
40 of the gyrotron cavity is a strong asset, since it allows a reduction in the investment cost of the
41 ancillary system. The former type of gyrotron is implemented in many present experiments. The
42 second approach requires the development of large broadband synthetic diamond windows,
43 which is now under way;
- 44 (c) in a reactor, two additional requirements may play an important role. First, the total power
45 delivered to the plasma may be large (e.g. on the order of many tens of MW in continuous wave
46 (CW) operation, implying a power per gyrotron in excess of 1 MW (in the range of 2 MW) as
47 discussed above. Secondly, in a reactor the electrical efficiency (defined as the ratio of the RF
48 output power to the electrical power to the tube) must be as high as possible to minimize the
49 recirculating power from the power plant. This consideration should also be a driver for the
50 R&D in the field of multi-stage depressed collectors, where an overall balance should be
51 performed by considering the electrical efficiency and the complexity of the collector design
52 and operation, the high-voltage power supply and reliability-availability-maintainability-
53 inspectability (RAMI) aspects. However, at the present state of EC systems, the data available
54 renders true RAMI studies difficult. At the end, the important point is the "expect" opinion on
55 the reliability and availability of gyrotrons, which will determine the number of gyrotrons to be
56 installed to deliver the required power (assuming a 100 % availability of a certain function).
57
58
59
60

2. Gyrotron interaction principle

In electron cyclotron masers (ECMs), the electromagnetic (EM) energy is radiated by relativistic electrons gyrating in an external longitudinal magnetic field with a perpendicular velocity v_{\perp} . The resonance condition between the periodic rotation of the electrons and the EM wave (TE mode) in the interaction circuit is according to eqs. (1) and (2)

$$\omega - k_{\parallel} v_{\parallel} = n\Omega_c, \quad n = 1, 2, \dots, \quad (5)$$

where k_{\parallel} is the characteristic axial wavenumber of the EM wave in the interaction structure, v_{\parallel} is the longitudinal electron drift velocity and $\Omega_c = \Omega_{c0}/\gamma$ is the relativistic electron cyclotron frequency. The relativistic Lorentz factor γ (eq. (4)) can be simply calculated from

$$\gamma = 1 + eV_b / m_0 c^2 \approx 1 + V_b / 511, \quad (6)$$

where V_b is the acceleration voltage of the electron beam in kV.

Gyrotrons are ECM oscillators, which mainly employ weakly relativistic electron beams ($V_b < 100$ kV, $\gamma < 1.2$) with high transverse momentum (velocity ratio $\alpha = v_{\perp}/v_{\parallel} = 1.2-1.5$) [15-21]. The wave vector of the EM wave in the cavity is almost transverse to the direction of the longitudinal magnetic field ($k_{\perp} \gg k_{\parallel}$ and the Doppler shift is small), resulting, according to eq. (5), in radiation near the electron cyclotron frequency or one of its harmonics:

$$\omega \cong n\Omega_c, \quad n = 1, 2, \dots \quad (7)$$

In cylindrical waveguide cavity gyrotrons the operating TE mode is close to cutoff ($v_{ph} = \omega/k_z \gg c$) and the frequency mismatch $\omega - n\Omega_c$ is small but positive in order to achieve correct phasing, i.e. keeping the azimuthal electron bunches in the retarding phase to transfer energy to the TE wave. The Doppler term $k_{\parallel}v_{\parallel}$ is of the order of the gain width and is small compared to the radiation frequency. The interaction efficiency is between 35 % and 40 %. The finite value of the minimum electron energy after the cavity allows the application of a retarding potential to the spent electron beam for recovery of beam power and thus for efficiency improvement (see Section 3.5).

The frequency of a gyrotron is approximately given by the cutoff frequency f_{cut} of the cavity mode:

$$f_{cut} \text{ (GHz)} = 95.4269 \chi_{m,n} / D \text{ (mm)} \quad (8)$$

where $\chi_{m,n}$ is the n^{th} root of the derivative of the corresponding Bessel function J'_m (TE_{mn} mode) and D is the cavity diameter. For millimeter (mm)-wave gyrotron cavities (e.g. 170 GHz) with a diffraction quality factor Q of approximately 1000, the exact operating frequency is only about 250 MHz higher than the cutoff frequency f_{cut} [22].

Gyrotrons are capable of producing very high-power radiation at cm, mm and sub-mm wavelengths [15-21], since the use of large cavity and output waveguide cross sections reduces wall losses as well as the danger of breakdown and permits the passage of large, high-power electron beams. In contrast to klystrons, the resonance frequency of a gyrotron cavity is not determined by the characteristic size, but by the strength of the magnetic field (see eqs. (2) and (7)). According to eq. (8), for a given frequency, operation in a high-order mode (determined by its eigenvalue $\chi_{m,n}$) with low Ohmic attenuation can be selected just by the cavity diameter. Since the Ohmic skin losses are proportional to $1/(\chi_{m,n}^2 - m^2)$, volume modes with $0.3 \lesssim m/\chi_{m,n} \lesssim 0.5$ are preferable.

3. Components of modern fusion gyrotrons

The schematic layout of a typical megawatt-class fusion gyrotron installation is shown in figure 1. The gyrotron tube is inserted into the warm bore hole of a superconducting magnet (SCM). The following sections briefly describe the functions of the various components and innovations that have been introduced during recent years [19-21].

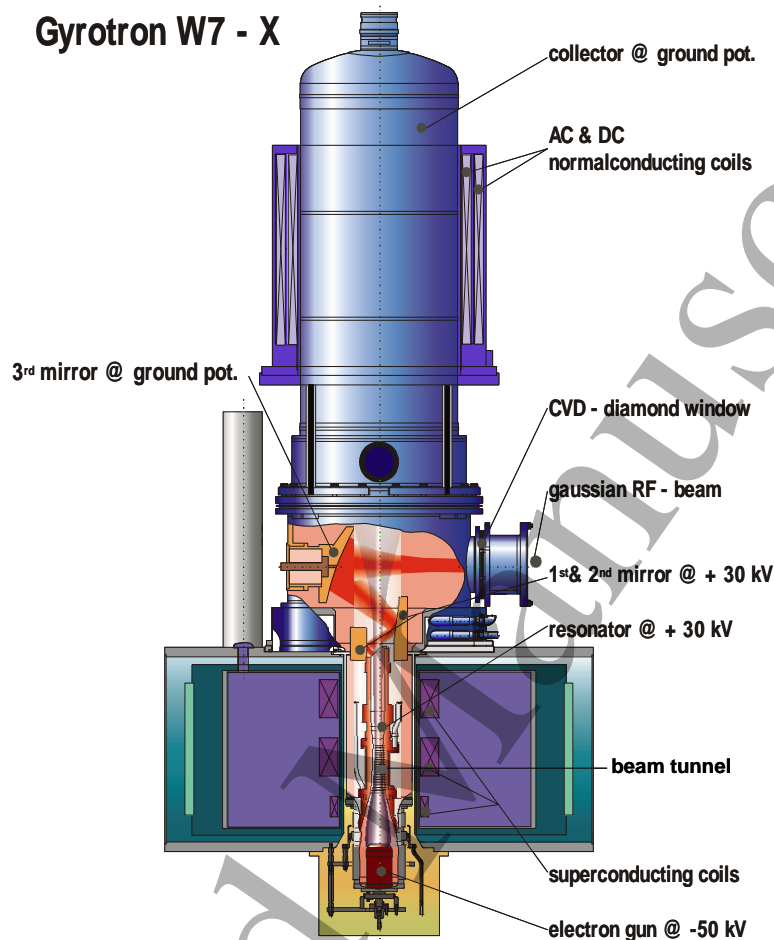


Figure 1. Schematic view of the 140 GHz, 1 MW, CW Thales gyrotron with superconducting magnet (SCM) utilized in the ECH system of the stellarator W7-X (© 2007 IEEE. Reprinted, with permission from [21] Thumm M 2014, IEEE Trans. on Plasma Science 42, 3, 590).

3.1 Magnetron injection gun and beam tunnel

In high-power fusion gyrotrons thermionic magnetron injection guns (MIGs) operating in the temperature limited (TL) current regime (Richardson-Dushman Law) with different electron flows (quasi-laminar, intermediate and regularly intersecting) have thus far been used most successfully [15,23]. This is in contrast to other types of microwave tubes such as klystrons and travelling-wave tubes, where electron guns operated under space-charge limited (SCL) conditions (Child-Langmuir Law) are used. In TL operation a non-zero electric field exists at the emitting surface and accelerates all electrons towards the anode. In this case the electron beam current I_{beam} is only weakly dependent on the acceleration voltage V_0 as a result of the Schottky effect, but the properties of the beam sensitively depend on the conditions of the emitting surface. The beam current is then adjusted by the temperature of the emitter. The characteristic feature of such MIGs is the emission of electrons in crossed electric and magnetic fields, forming an electron beam, which contains cyclotron motion. Impregnated tungsten dispenser or lanthanum hexaboride (LaB_6) cathodes are being employed in diode-type (two electrodes) or triode-type (three electrodes) guns (see figure 2). Triode guns with a modulation anode offer the possibility of variation of the electron beam velocity ratio α (pitch factor) in the interaction cavity and

of requiring only a low power high-voltage (HV) modulator for efficient modulation of the output power. Simulation calculations on the interaction in gyrotron cavities show that the efficiency of RF generation decreases as the distribution of the velocity components of the electrons in the electron beam broadens. Various measurements showed velocity spreads $\delta v_{\perp} = (v_{\perp \max} - v_{\perp \min})/2v_{\perp} = 15\text{-}30\%$ ($\delta v_{\perp \text{rms}} \cong 6\text{-}12\%$) [15,24].

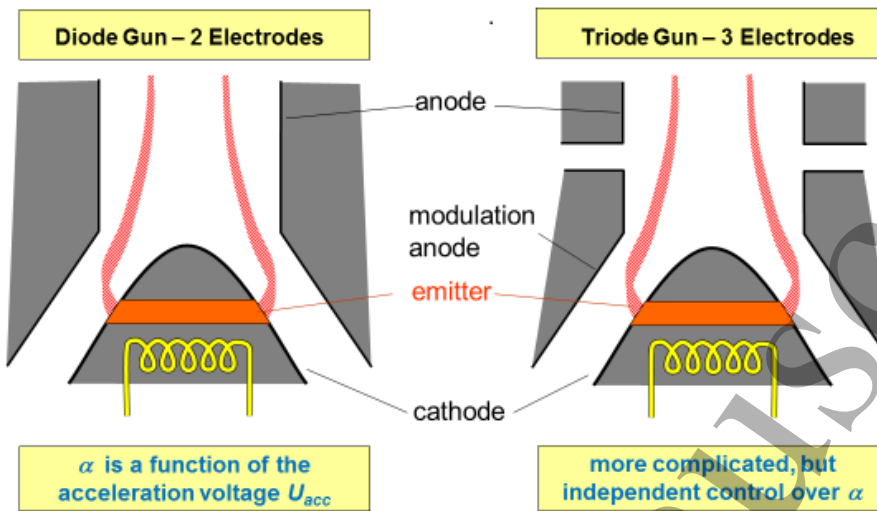


Figure 2. Two different types of magnetron injection guns (MIGs) for gyrotrons, diode gun (left) and triode gun (right). The pitch factor α of the electron beam in the cavity is determined by the magnetic mirror ratio between the MIG and the cavity, and the acceleration voltage. The triode MIG has the merit that α is controlled by the modulation-anode voltage, independently with respect to other parameters.

The possible sources of velocity spread, which have been suggested include: roughness of the emitter surface, spread of initial electron velocity at the cathode (both energy and direction), non-axisymmetric behaviour (non-uniform work function around the emitter ring, thermal inhomogeneities, misalignment of electrodes and magnetic field), non-adiabatic behavior, instabilities during transport of the electron beam through the beam tunnel (compression zone) to the cavity and space charge effects due to reflected electrons trapped between the magnetic mirror and the cathode, which also may raise the average pitch factor [25,26]. Proper shaping of the neighboring parts of the emitter ring or/and anti-emission coatings are necessary. The angle between the emitter surface and the magnetic field determines the characteristics of the trajectories. Quasi-laminar beams show the lowest values of velocity spread. For clean excitation of the operating mode, the thickness of the electron beam in the cavity should be smaller than approximately $\lambda/5$, where λ is the free-space wavelength. Optimum MIG designs are being achieved using advanced trajectory and particle-in-cell (PIC) codes.

The beam tunnel is especially prone to parasitic gyrotron-type oscillations, since the perpendicular energy of the electrons increases on the way from the emitter ring to the cavity. Azimuthally symmetric high-order TE_{0n} gyro-backward waves are the most dangerous source of parasitic oscillations, since it is difficult to attenuate them, especially in high-electron-current MW gyrotrons [27,28]. Several improved beam-tunnel damping structures have been developed to avoid unwanted oscillations:

- Non-axisymmetric conical metallic structures (IAP) [19]
- Conical silicon carbide (pure SiC) structures. SiC is a good mm-wave absorber and a weak semiconductor to avoid static charges (QST) [29]
- Conical alternating stack of BeO/SiC(60/40) ceramic damping rings and copper rings. The copper rings are indented with a slot depth of about $\lambda/4$ in order to cut off azimuthal RF currents and to break the azimuthal symmetry. The number, width and periodicity of the indentations can vary irregularly (KIT). Such a structure can also be considered as a grating with many different grating constants. This complicates the formation of a resonant field structure and effectively damps $TE_{m,n}$ modes, in particular, symmetric TE_{0n} modes [27].

3.2 Cavity

The gyrotron interaction circuit, the cavity, is a straight cylindrical resonator with a radius down taper below the cutoff radius of the operating mode at the input of the electron beam and a non-linear up taper as mm-wave output [15-22]. Mode conversion to unwanted spurious modes is strongly reduced by the use of curved transitions between the cylindrical and taper sections and an optimized radius contour of the output taper (see figure 3). The cavity is placed at the position of the maximum magnetic field. In order to raise the gyrotron power to the MW level, the cavity modes have changed over the past 35 years from low-order modes (e.g. TE_{02} , with cavity radius $\approx \lambda$) to very high-order volume modes, e.g. $TE_{25,10}$, $TE_{31,11}$ and $TE_{32,9}$, with cavity radius $\approx 10\lambda$, for the Russian, Japanese and European ITER gyrotrons, respectively (see figure 4), rotating in the same direction as the gyrating electrons

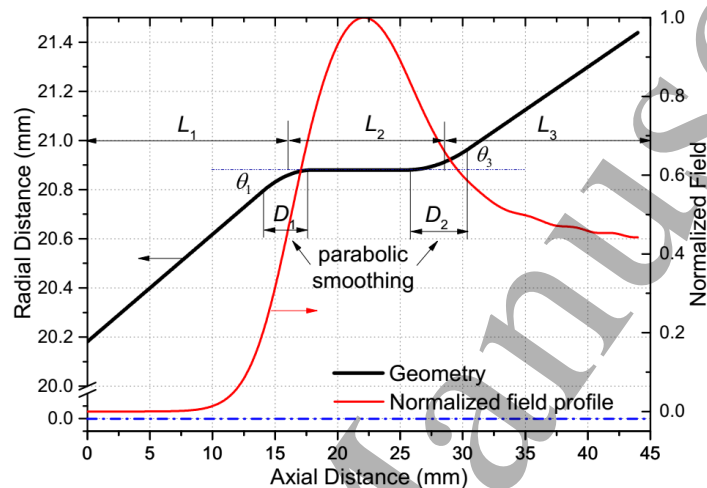


Figure 3. Radius contour of an open-ended circular waveguide gyrotron cavity with normalized profile of the magnitude of the electric field.

(co-rotating). Diffractive quality factors are between 1000 and 1500 [22]. Stable and efficient gyrotron operation in such high-order modes with very dense competing mode spectra became feasible due to the use of high-quality helical electron beams with $\alpha = 1.2 - 1.4$, generated by improved MIGs, and the development of advanced self-consistent, time-dependent multi-mode cavity interaction simulation codes needed for understanding the problems associated with mode competition and start-up scenarios.

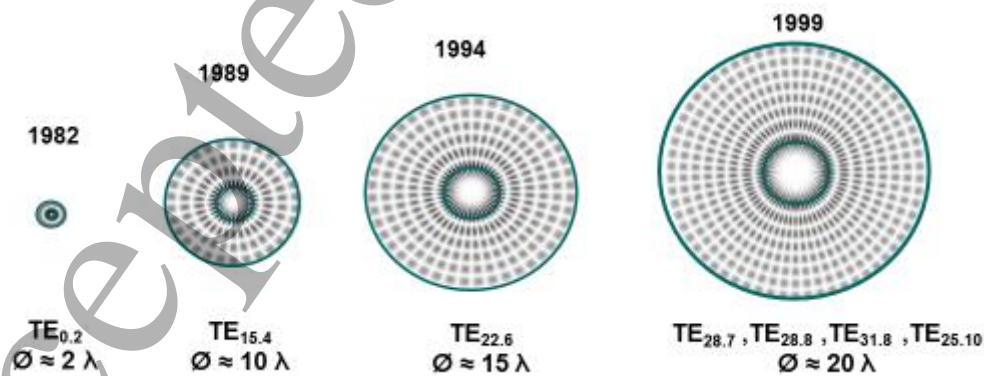


Figure 4. Schematic intensity contours of typical cavity modes and comparison of cavity sizes during the different development steps of gyrotrons for fusion plasma heating. The patterns are plotted for azimuthally standing modes, whereas the actual mode is a rotating one.

Megawatt-class gyrotrons employ electron beams with 70 to 80 keV electron energy and 45 to 40 A beam current. The annular electron beam is located on the first maximum of the cavity mode electric

1
2
3 field leading to interaction efficiencies between 35 % and 40 %. The cavity material is OFHC copper
4 or dispersion strengthened copper (Glidcop) with improved thermo-mechanical performance. Porous
5 structure or mini-channel cooling is employed resulting in acceptable peak Ohmic wall losses of
6 approximately 2 and 2.5 kW/cm², respectively, resulting in cavity expansions (frequency down chirps)
7 of 0.1 to 0.25 %.

8 9 3.3 Quasi-optical output coupler

10
11 For 1 MW CW fusion gyrotrons the implementation of an output coupling approach is required that
12 separates the spent electron beam from the outgoing RF beam in order to increase the collector electron
13 beam interception area. It is the short-wavelength, high-output-power and the rotating asymmetric high-
14 order cavity mode of such tubes, which required quasi-optical (q.o.) mode conversion concepts (first in
15 Russia [30]).

16
17 The q.o. mode converter is a part of the internal EM system of the gyrotron, which also includes the
18 cavity and the up taper (figure 1). Radial output coupling of the RF power into the linearly polarized
19 fundamental Gaussian (TEM_{0,0}) free-space mode has several significant advantages for high-power
20 operation. Q.o. gyrotron mode transducers generating a wave beam consist of an asymmetrical
21 waveguide opening (launcher) with a specific feeding waveguide and several focusing and phase
22 correcting mirrors (figure 1) [31].

23
24 At the aperture of conventional cylindrical waveguide launchers, there exists an approximately uniform
25 field distribution in the axial and azimuthal directions, leading to high-diffraction losses of about 20%.
26 Stray radiation in the gyrotron is one of the critical factors affecting pulse-length extension. A pre-
27 bunching q.o. launcher, which reduces the stray radiation was firstly reported in 1991 [32]. To form a
28 Gaussian field distribution at the launcher output, essentially eight adjacent modes are generated by
29 small periodic helical perturbations on the inner surface of the launcher wall [31-33]. Thereby the
30 diffraction loss was reduced from 20% to < 5%. In the 2000's, the diffraction loss was reduced further.
31 In the 140 GHz gyrotron for W7-X, in which an analytically-designed mode converter has been
32 installed, a measured internal loss of only ~ 2% was attained [34], which contributed to long-pulse
33 operation of the tube. Intensity profile measurements of the output beam were performed by inserting a
34 PVC target plate into the RF beam and measuring the temperature profile with an IR-camera. RF beam
35 reconstruction using a phase retrieval code yielded a Gaussian beam content of around 97.5% [34].

36
37 More recently, numerical methods for launcher optimization were developed [35-38]. In the code
38 developed in [35] the helical surface deformation is optimized such that many modes are excited and
39 combined to form the Gaussian beam at the launcher output. For example, 99.5% of the radiated power
40 was received by the first mirror in the Japanese 170 GHz gyrotron. In this case, the initial TE_{31,8} mode
41 is distributed among 15 modes to form the Gaussian intensity distribution.

42
43 Reduced launcher length is obtained by an internal line of mirrors with mode-converting and phase-
44 correction non-quadratic surface contour functions optimized by iteratively solving the scalar diffraction
45 integral equation [36, 37]. The validation of such improved launchers has been performed using 3D full-
46 wave EM field solvers (e.g. SURF3D [38]). Combination of helical-like and mirror-type wall
47 perturbations (hybrid-type launchers) may even increase the output mode purity [39]. These techniques
48 have been extended to launchers that work for many frequencies. High conversion efficiencies of over
49 96% for several modes have been reported, which opens the way for high-efficiency multi-frequency
50 gyrotrons (see Section 5).

51 52 3.4 Synthetic diamond output window

53
54 In order to select the appropriate concept for the development of 1 MW, CW mm-wave windows one
55 has to compare the thermo-physical, mechanical and dielectric parameters of possible window materials
56 related to the load-failure resistance and the power-transmission capacity at different temperatures. The
57 features of beryllia, boron nitride, silicon nitride, sapphire, Au-doped silicon, silicon carbide and CVD
58 diamond are compared in [40].
59
60

The evaluation of BeO, BN, Si₃N₄, sapphire and SiC clearly shows that there is no chance to use these dielectrics as an edge-cooled, single-disk 1 MW, CW window at room temperatures. Experiments at CPI in the USA and at NIFS and JAEA in Japan confirmed, that even a double-disk FC75-face-cooled sapphire window has a CW-power limit around 0.3-0.4 MW [40 and references given there] Nevertheless, these materials are widely used in lower power gyrotrons and pulsed operation. At present, polycrystalline chemical vapour deposition (CVD) diamond is the only material for simple, edge-cooled (water) single-disk MW-class CW gyrotron windows [41-43]. Current CVD capabilities allow samples of up to 140 mm diameter and 2.5 mm thickness (570 carat). There are only three suppliers: Element Six in the Netherlands, Diamond Materials in Germany and II-VI Advanced Materials in the USA. CVD diamond is attractive due to its good mechanical properties (bending strength: $\sigma_B = 400$ MPa), very small thermal expansion ($\alpha' = 10^{-6}/K^{-1}$), modest dielectric constant ($\epsilon_r' = 5.67 \pm 0.01$), low mm-wave attenuation ($\tan \delta \approx 2 \cdot 10^{-5}$) and very high thermal conductivity ($k = 1900$ W/mK at room temperature). Nuclear irradiation with $<10^{21}$ neutrons/m² and 0.8 Gy/s γ /X-rays is acceptable and brazing technologies are available. The transmission frequencies of a simple, standard single-disk window are

$$f = nc/2d \sqrt{\epsilon_r'} \quad (n = 1, 2, 3, \dots), \quad (9)$$

where d is the thickness. Eq. (9) leads to $d = n \lambda/2$, where λ is the wavelength in the window material. For example, the thickness of a synthetic diamond 170 GHz (140 GHz) gyrotron window disk with approximately 100 mm diameter is $d = 1.852$ mm ($d = 1.799$ mm), corresponding to $n = 5$ ($n = 4$). This thickness can safely handle the vacuum pressure inside the gyrotron. It could also be used as a vacuum window at the plasma device and can withstand up to 2 bar absolute pressure difference, as required by nuclear safety.

Cu-Au-, Cu-Ag- and Al-braze processes are utilized by the different tube companies. When using an Al-braze, the baking temperature of the gyrotron has to be reduced to 450 °C and the corrosion inhibitor CC15 must be added to the cooling water to prevent corrosion. In the Japanese tubes, the bonding part is coated with a copper plating, and pure water is used as coolant.

3.5 Single-stage depressed collector

The electronic interaction efficiency η_{osc} of the annular, helical electron beam in a gyrotron cavity is between 35 and 40 % so that the remaining power of the beam after interaction (spent electron beam) amounts to 65 - 60 % of the initial beam power. Fortunately, the energy distribution after the electron cyclotron interaction in the cavity has a clear minimum value as discussed in Section 2. By applying a static retarding voltage V_{dep} between cavity and collector, the spent beam loses its power, which is recovered by the power supply (see figure 5). The total RF generation efficiency is

$$\eta_{total} = \eta_{osc} V_b / (V_b - V_{dep}). \quad (10)$$

Here, V_b is the beam voltage. The retarding voltage V_{dep} corresponds to the minimum energy of the spent electron beam. For $\eta_{osc} = 35\%$, $V_{dep} = 30$ kV and $V_b = 80$ kV, this results to $\eta_{total} = 56\%$ [44,45]. The merits of depressed collectors are: The required voltage of the main power supply is significantly reduced (e.g., from 80 kV to 50 kV) and the energy of the spent electron beam and thus the collector heat load is significantly lowered which allows the reduction of the collector size and/or an increase in the gyrotron reliability as well as a reduction of the required capacities of the cooling and power supply systems. In addition, energy and power of the generated X-rays are less.

There are two gyrotron design modifications used for single-stage depressed collectors (SDCs) differing essentially by the position of the DC break insulator needed to apply the depression voltage (see figure 5) [46]. In the gyrotron design with a ceramic insulator located above the SCM ("top" version), the gyrotron body and outer jacket is held at high positive voltage and has to be electrically insulated from the warm bore of the SCM. In the design with a ceramic insulator located below the SCM (see figure 1), the gyrotron body is at high positive voltage, but the jacket is grounded and does not need any insulation between gyrotron and magnet. In the "bottom" version the ceramic insulator has a smaller diameter facilitating the system for ceramic cooling. On the other hand, this "bottom" version has some disadvantages like lower acceptable depression voltage and correspondingly lower possible rise in the

total efficiency using a SDC (the difference in efficiency can be about 3% percentage points). Another disadvantage is that the anode-cavity unit forms a rather long interior cantilever that is sensitive to mechanical shocks and vibrations and needs special care under transportation.

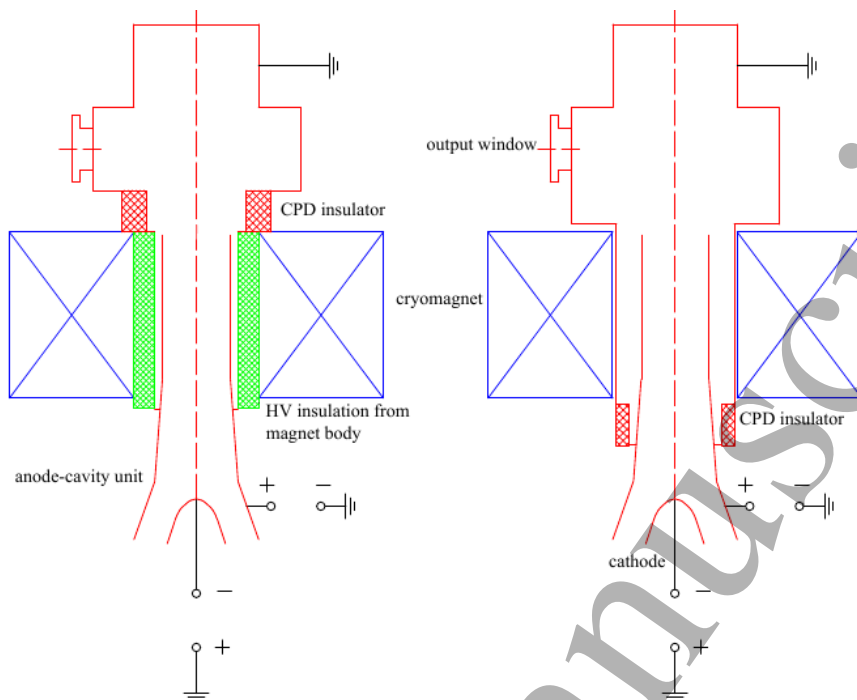


Figure 5. Two types of insulation of single-stage depressed collectors (SDCs) [46]. Left: Upper collector potential depression (CPD) insulator. Right: Lower CPD insulator. In both cases the collector is grounded and the tube body is positively biased. As a result, the voltage of the main power supply can be reduced keeping the initial electron beam energy the same.

3.6 Auxiliary components

3.6.1 Sweeping of spent electron beam in the collector

Vertical magnetic field sweeping systems (VFSSs) have become a standard technique to keep the time-averaged heat dissipation from the spent electron beam at the collector within technically acceptable values ($< 500 \text{ W/cm}^2$). If the collector diameter is constant, such collectors operate close to the technological limit and are a high-risk component with a small safety margin. To address this problem, KIT Karlsruhe in collaboration with IPP Greifswald investigated and optimized a combined 7 Hz VFSS and a 50 Hz transverse field sweeping system (TFSS) for the 140 GHz W7-X gyrotrons. The TFSS consists of 3 pairs of TF-coils, which are powered by a conventional 3-phase AC-supply thus generating a transverse field, which rotates at 50 Hz [47]. At the position of the coils the collector is made of stainless steel in order to reduce the influence of eddy currents. By proper tuning of both systems an almost perfectly flat power deposition profile along the collector area was obtained. The peak loading is reduced by about a factor of 1.6 as compared to VFSS alone [48]. Other possibilities are to employ collectors with an optimized inner radius profile or to utilize an advanced magnet current modulation scheme for the VFSSs or TFSS [47], to lower the maximum surface loading.

3.6.2 Superconducting gyrotron magnet

Since the gyrotron is an ECM, it absolutely needs a magnet which according to eq. (1) for mm-wave gyrotrons must be a SCM ($B \approx 6.7 \text{ T}$ for 170 GHz). Russian gyrotrons use a magnetic field profile which is symmetric towards both the MIG and collector. Only a weak normal conducting gun coil is employed to slightly correct the magnetic field in the cathode emitter area. In contrast to this, European, Japanese and US tubes operate in a SCM, where a bucking coil in the beam tunnel region lowers the magnetic field in order to reduce the distance between electron emitter and the cavity center. In this case, the gun coil is also superconducting and integrated into the cryostat. The material of the wires is NbTi, which is cooled down only by a refrigerator. These SCMs are maintenance free in principle, and have generally

1
2
3 been free of operational problems. The Russian and Japanese 170 GHz ITER gyrotrons both operate in
4 cryogen-free JASTEC magnets, whereas the European tube is equipped with a cryogen-free SCM
5 manufactured by CRYOGENIC in UK.
6

7 *3.6.3 Dummy load and RF measurement system*

8 Essential for the development of efficient fusion gyrotrons is a high-power diagnostic system enabling
9 measurement of the output power, frequency- and mode spectra and output mode purity. In a gyrotron
10 test facility, a high-power dummy load is an important apparatus. At present, water-cooled metal vessels,
11 whose inner surfaces are coated by an absorbing dielectric material [49,50], or pure stainless steel
12 vessels are commonly used [46]. Water flow rate and input-output water temperature difference
13 determine the measured power level. The RF beam is injected quasi-optically and absorbed during multi-
14 reflections in the vessel. By rotating the RF beam with a mirror, the averaged power density is reduced
15 on the surface. 1 MW-class operation has proved to be feasible. Sometimes a so-called pre-load absorbs
16 the RF power reflected by the dummy load [29]. Arc detectors at the gyrotron output window, at
17 corrugated surface polarizers and at the input of the dummy load guarantee fast switch-off in case of
18 arcing. For first tube tests at short pulse duration (ms-range) special short-pulse calorimeters (ballistic
19 or with coolant flow) are utilized. Time-dependent frequency spectra are measured by parallel filter-
20 bank spectrum analyzers, frequency-time analyzers or pulse spectrum analysis (PSA) systems providing
21 spectrograms [51]. Mode-purity measurements are being performed using thermographic imaging
22 (infrared camera) of the output beam pattern on a target plate at different distances from the window.
23 Beam reconstruction employing phase retrieval codes allows a determination of the fundamental
24 Gaussian mode content [52].
25
26
27

28 **4. Megawatt-class fusion gyrotrons**

29
30
31 Worldwide, there are four microwave-tube companies, which manufacture megawatt-class gyrotrons
32 for fusion research: Communications & Power Industries (CPI) in Palo Alto, USA; GYCOM in Nizhny
33 Novgorod, Russia, in collaboration with the Institute of Applied Physics (IAP); Thales – Microwave &
34 Imaging Subsystems (THALES) in Velizy, France, in collaboration with the European Gyrotron
35 Consortium (EGYC); and Canon Electron Tubes & Devices Co., Ltd. (CETD, prior to October 2018,
36 Toshiba Electron Tubes & Devices Co., Ltd. TETD), Otawara, Japan, in collaboration with the National
37 Institutes for Quantum and Radiological Science and Technology (QST). The members of EGYC are:
38 KIT, Germany; SPC, Switzerland; HELLAS, Greece, CNR and ENEA, Italy.
39

40 *4.1 ITER Gyrotrons*

41 *4.1.1 Configuration of ITER gyrotron system for 20 MW ECH&CD*

42
43
44 For ITER a 20 MW (power delivered to the plasma), 170 GHz ECH&CD system is planned for plasma
45 heating to self-ignition and non-inductive current drive for plasma confinement and control of NTMs
46 [8,53,54]. For this purpose, the development of long-pulse 1 MW 170 GHz gyrotrons has been carried
47 out since the ITER EDA (Engineering Design Activities) phase that started in 1995. 24 MW source RF
48 power is being prepared, taking into account 4 MW transmission losses (16.7 %). 8 MW power
49 generation is allocated for the two parties of Russia and Japan, respectively, 6 MW for the EU and
50 2 MW for India. CW operation should be considered in the designs. For ITER, a 4-step operation
51 scenario is considered: “First plasma (FP)”, “Pre-Fusion Power Operation I (PFPO-I)”, “Pre-Fusion
52 Power Operation II (PFPO-II)” and “Fusion Power Operation (DT)”. The available heating power will
53 be increased gradually for each step by adding Ion Cyclotron Heating (ICH) and Negative Ion Neutral
54 Beam Injection (NNBI). EC power injection is expected from the first plasma initiation in 2025. In the
55 FP phase, 8 gyrotrons will be used to inject 6.7 MW. After the “PFPO-I” phase, full 20 MW EC power
56 injection is expected. In addition, there is a possible strategy to apply dual-frequency gyrotrons
57 (170 GHz/104 GHz) in the “PFPO-I” phase for H-mode studies at reduced toroidal magnetic field
58 (1.8 T). Another role of the ECH&CD system is MHD mode suppression, in particular Neoclassical
59 Tearing Modes (NTMs). For this purpose, up to 5 kHz power modulation is required (full on/off power
60 modulation is expected).

In figure 6 the configuration of the ITER and RF building is illustrated. Twenty four 1 MW gyrotrons are placed in the RF building. An evacuated corrugated HE₁₁ waveguide is connected to each gyrotron via a matching optics unit (MOU), from where the power is transmitted to the ITER torus. There are two types of launchers. One is a launcher installed in an equatorial port for plasma ignition and current drive, and the other four launchers are installed in upper vessel ports for plasma initiation and MHD control. The routing of mm-wave power transmission to the different launchers is selected using waveguide switches. In figures 7 and 8, different views of the RF building are shown. The main power supplies are installed on the 1st floor. On the 2nd floor, the body power supplies and anode power supplies (for the eight QST gyrotrons) are placed. The 3rd floor is the location of all the 24 gyrotrons. Gyrotrons are sensitive to stray magnetic fields, since those influence the electron beam trajectories in the tubes. The stray magnetic field of the ITER poloidal field and the plasma current is estimated to be within an acceptable level (2 Gauss in radial direction). If necessary (especially because of the stray magnetic field of the gyrotron SCMs), compensation coils may have to be installed at the gyrotrons.

The specifications for the ITER gyrotrons are as follows:

- Power and HE₁₁-mode purity at the output of the MOU: ≥ 0.96 MW and > 95 %, respectively
- RF power generation efficiency: ≥ 50 %
- Pulse duration: gyrotron and auxiliaries have to be designed for 3200-s pulses, the acceptance tests are being performed at 1000-s pulse duration
- Reliability: ≥ 95 % defined on 20 full-power pulses with 500-s duration.

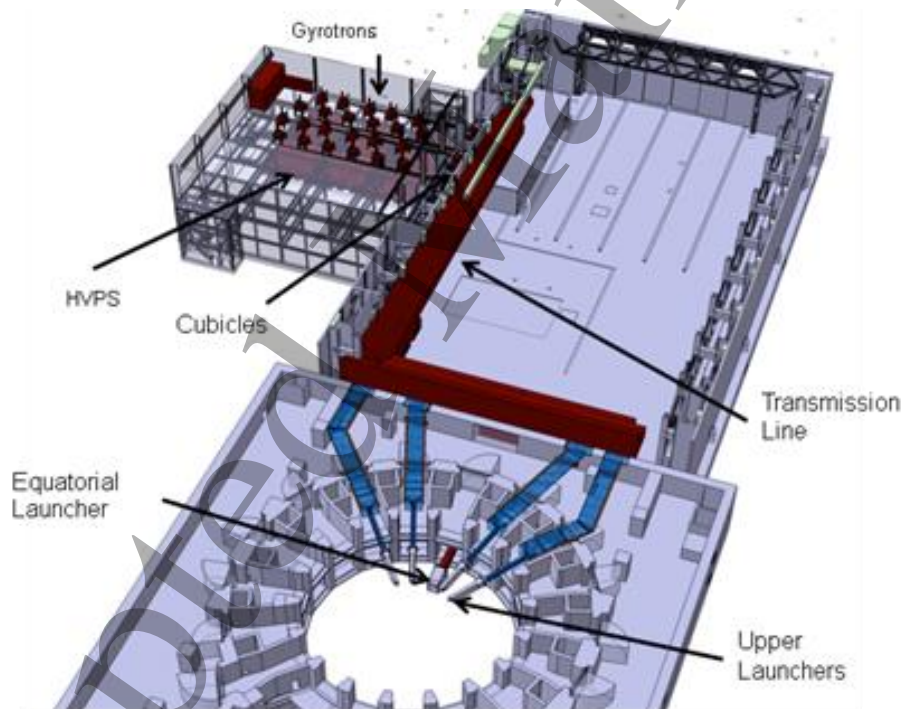


Figure 6. Configuration of ITER building and RF building where the 24 gyrotrons are installed. Long evacuated corrugated waveguides transmit the mm-wave power in the HE₁₁-hybrid mode to the launchers at the torus. The ECH&CD system has one equatorial launcher, connected with 24 waveguides, and four upper port launchers, each connected with eight waveguides. Power routing is performed by waveguide switches.



Figure 7. Vertical view of the ITER RF building. The main power supplies are placed on the L1 Ground Level). On level L2, the body and anode (for the JA gyrotrons) power supplies are located. On L3, the gyrotrons and their ancillary facilities, such as superconducting magnets (SCMs), are installed.

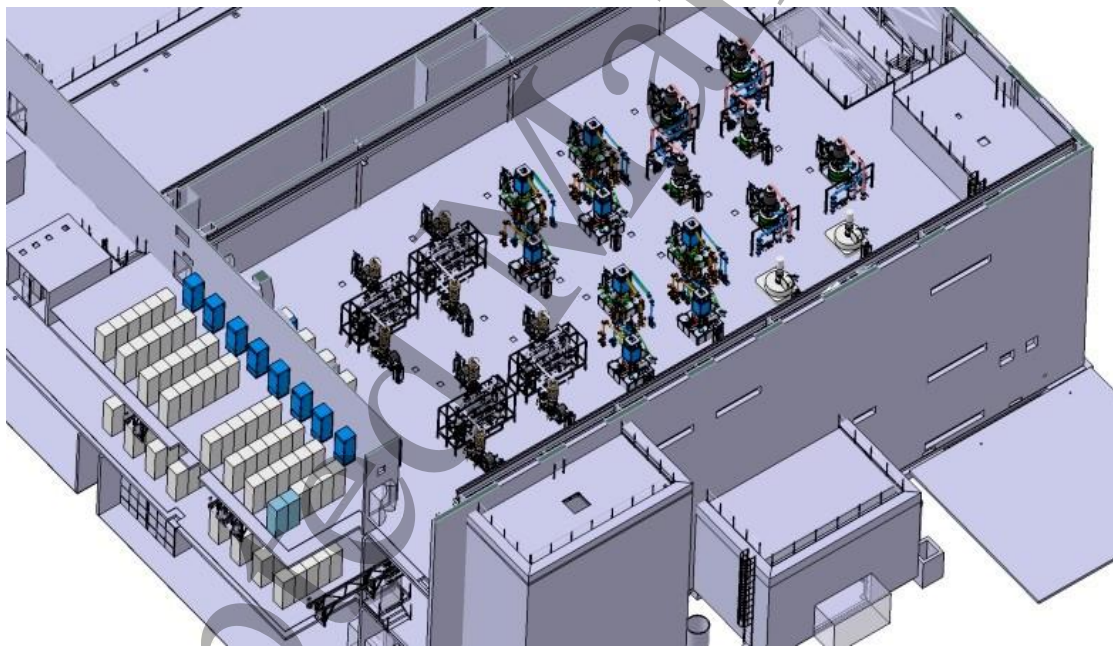


Figure 8. View of level L3 of the ITER RF building where the 24 gyrotrons are placed.

4.1.2 Japanese ITER gyrotron

QST is the Japanese Domestic Agency (JADA) of the ITER project. QST has the responsibility for the procurement of eight sets of 1 MW, 170 GHz gyrotron SCM, gyrotron stand, MOU and anode power supply for triode MIG operation. A photo and a technical drawing of the gyrotron are shown in figure 9. A photo of the gyrotron system composed of the gyrotron, MOU, oil tank, SCM and gyrotron stand is shown in figure 10. The design of the main parts was carried out at QST (formerly JAEA) and fabricated by industry (CETD). All test experiments have been performed by QST at its RF Test Stand (RFTS). The gyrotron MIG is a triode. Initially, the operating cavity mode $TE_{31,8}$ was selected

[29,55,56]. The mini-channel cooled Glidcop cavity has an inner radius of 17.9 mm. In the beam tunnel (between the MIG and cavity), a silicon carbide cone is installed to suppress parasitic oscillations before the cavity. The material used for the ceramic cylinder between the collector and tube body, where the retarding potential is applied for depressed collector operation (top version insulator, see 3.5), is silicon nitride (Kyocera SN 238), which is used because this ceramic cylinder also acts as “relief window”. SN 238 is mechanically tough and has a reasonably low loss tangent ($\sim 2.0 \times 10^{-4}$). The collector uses vertical electron beam sweeping (VFSS). After successful demonstration of 1 MW quasi-CW operation, the radial cavity mode number was raised from 8 to 11 obtain a greater margin for the cavity wall heat load caused by Ohmic losses (20.87 mm cavity radius), which enables an increase in power, and maintains the same electron beam radius. In addition, the $TE_{31,11}$ cavity mode has significant advantages for step-tunable gyrotron operation as discussed in Section 5. The generated power is converted to a Gaussian beam using an in-waveguide mode converter (launcher) followed by four mirrors inside the gyrotron. An edge-cooled synthetic diamond window is used at the tube output. As for the RFTS, the main power supply has a capability of 90 kV/50 A in CW operation. Switching of the DC power delivery to the gyrotron is done using a chain of IGBTs (Insulated Gate Bipolar Transistors), which has been in operation since 1998 without major trouble. The cryogen-free type SCM (JASTEC), with a 240-mm-diameter room temperature bore hole, is cooled by a refrigerator.

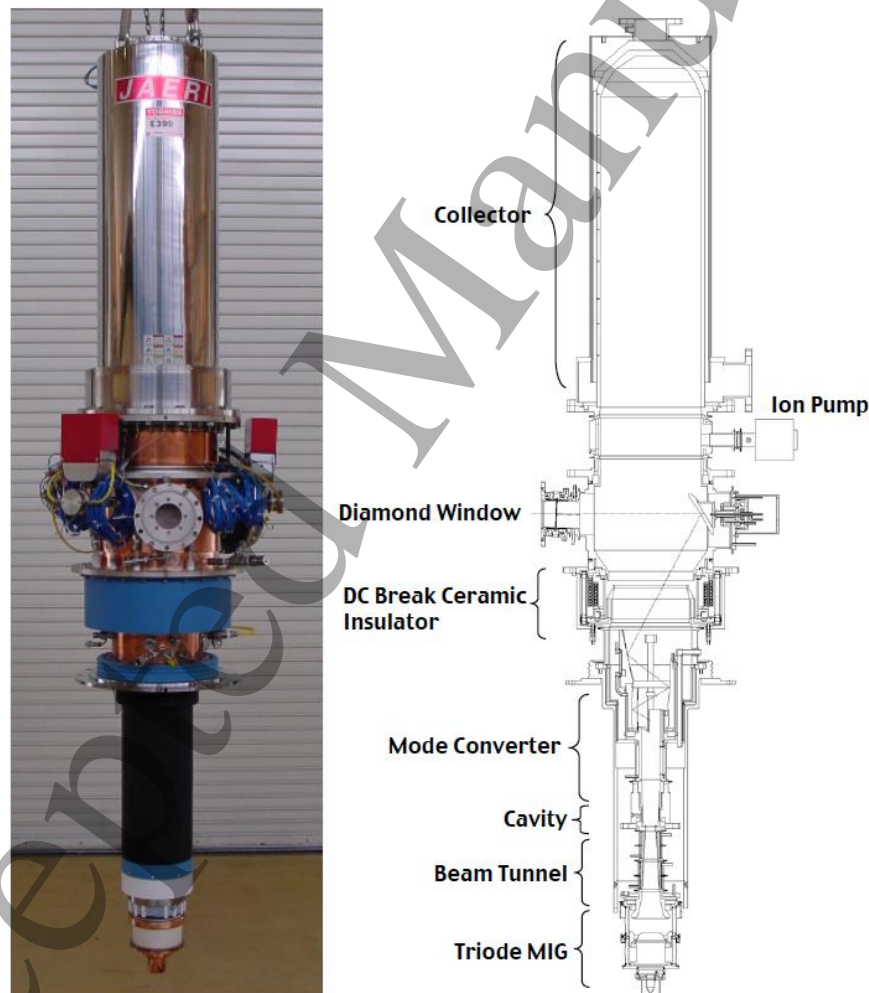


Figure 9. Photo and technical drawing of the Japanese 170 GHz ITER gyrotron.



Figure 10. Photo of the Japanese 170 GHz ITER gyrotron system with SCM, MOU and oil tank on the gyrotron stand.

(a) High efficiency long-pulse operation

Using the flexibility offered by the triode MIG, optimized operation parameters can be selected during tube operation by controlling both the magnetic field, B_c , in the cavity and the anode voltage, V_{ak} [57-59]. Here, the B_c determines the frequency mismatch parameter ($\Delta = \omega - \Omega_c = \omega - eB_c/m\gamma$) and the anode voltage, V_{ak} , determines the pitch factor of the electron beam. For example, B_c was scanned during the operation and a change of output power was monitored keeping the beam voltage V_b (corresponds to γ) constant. Figure 11 shows the B_c dependence of the output power. The arrows indicate the direction of the B_c scanning during the oscillation. As B_c decreases (Δ decreases), the power increases. After the plateau, the oscillation mode switches from $TE_{31,8}$ to $TE_{30,8}$. Then, B_c is increased again. The oscillation of the $TE_{30,8}$ mode remains until $B_c = 6.7$ T, then the operating mode switches to $TE_{31,8}$ again. The gap between $B_c = 6.645$ T \sim 6.7 T corresponds to the “hard excitation region”. B_c scanning at various V_{ak} gives the dependence of the output power contour as shown in figure 12. The vertical axis is V_{ak} and the abscissa is B_c . With the control of B_c and V_{ak} , the maximum power operation point can be found taking an arbitrary route in this parameter map. This is the merit of a triode MIG, which is particularly useful if even higher cavity modes are utilized whose mode competition is even more significant. As a result, stable 1 hr oscillation was demonstrated at an output power of 0.8 MW (57% efficiency), and 1.0 MW (800s) with 55 % efficiency employing a single-stage depressed collector. The maximum efficiency was 60 % at 0.6 MW, which is the highest value for high frequency gyrotrons (>100 GHz). The Gaussian output-mode purity was approximately 96 %. The optimum operation point was found in the deep hard excitation region, which was attained by active control of the magnetic field and the pitch factor of the electron beam. The vacuum level remained constant during long-pulse operation.

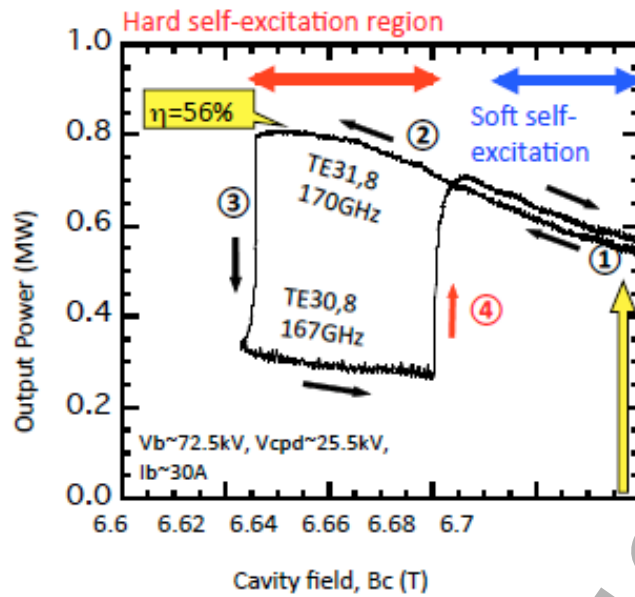


Figure 11. Output power and oscillating cavity mode vs cavity magnetic field [57]. From operating point ① B_c is decreased while remaining the $TE_{31,8}$ mode oscillation. At $B_c = 6.642$ T, the oscillation switches to the $TE_{30,8}$ mode (③). Then B_c is increased. At $B_c = 6.7$ T, the $TE_{30,8}$ mode oscillation switches back to the $TE_{31,8}$ mode. The region of $B_c = 6.642$ T \sim 6.7 T corresponds to the “hard self-excitation region”.

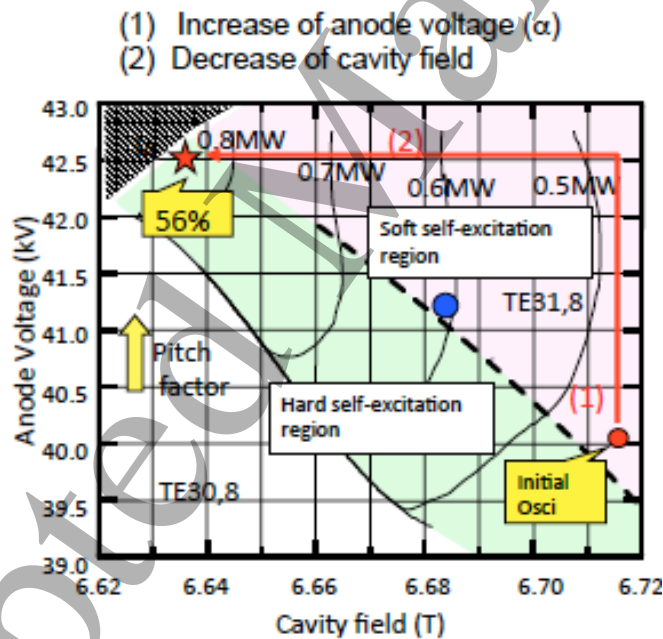


Figure 12. Power contours for 170 GHz $TE_{31,8}$ -mode oscillation versus anode voltage and cavity magnetic field at $V_b \sim -72.5$ kV and $I_b = 30$ A [57].

(b) Power modulation

Full on/off power modulation with a repetition frequency of up to 5 kHz in continuous operation is required for MHD control of ITER. If the power is modulated using an IGBT switch in the main cathode voltage power supply, the heat load on the switch becomes significant. To realize CW power modulation, a full-current modulation of the electron beam is employed using modulation-anode-voltage switching of the triode MIG. However, if the modulation is done with a finite-current modulation rather large electron beam power flows into the collector. Therefore, it is important to cut the electron current

to zero in the non-RF-power generation phase by decreasing V_{ak} to zero. Then the averaged collector heat load can be significantly suppressed. To realize the full-current modulation, the power supply system was newly developed as shown in figure 13. In the case of oscillation phase, voltage is applied between the modulation-anode and cathode by setting switch SW1 closed and SW2 open.

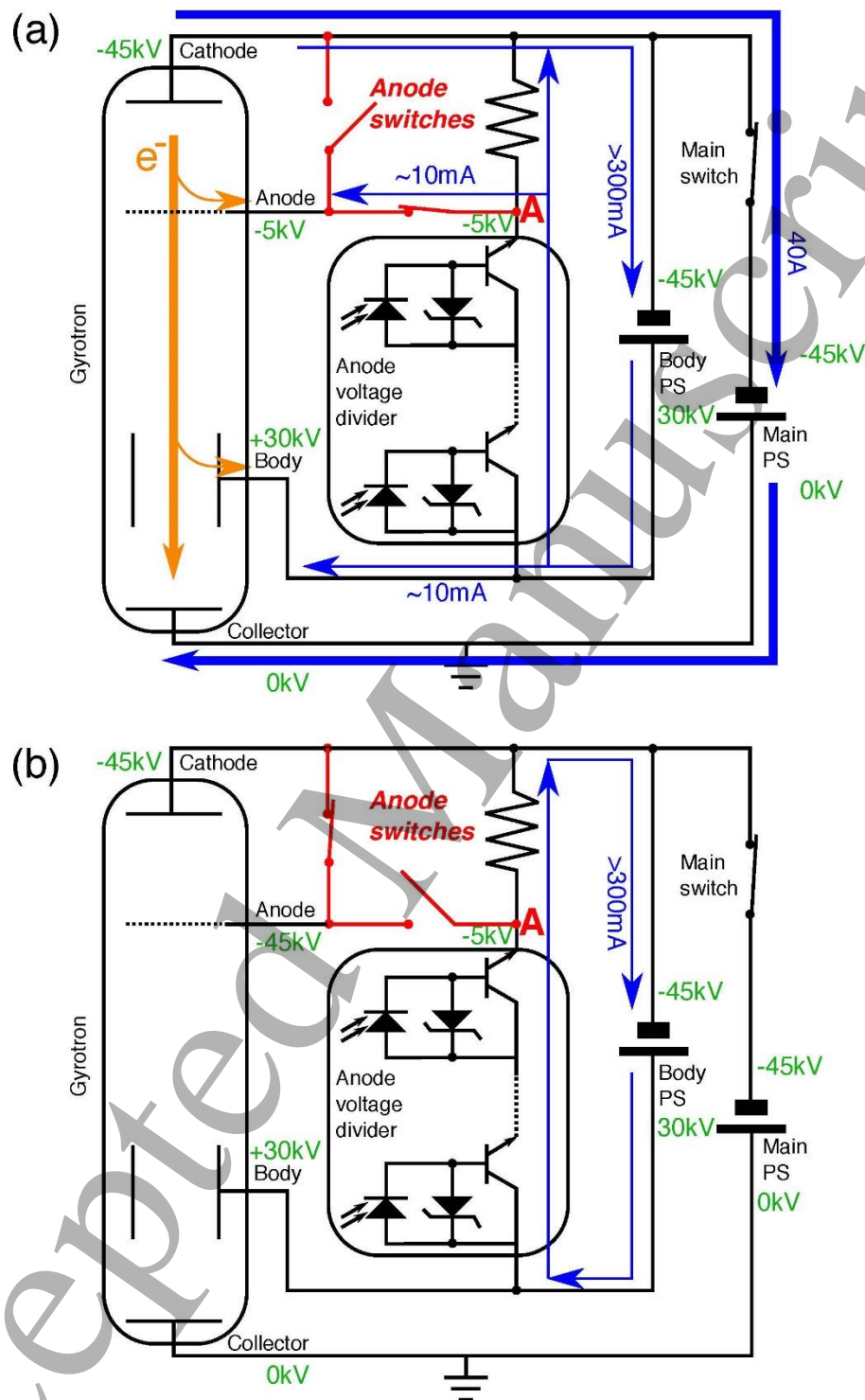


Figure 13. Configuration of power supply with double modulation-anode switches to enable high-frequency power modulation [60]. Rectangular current modulation is achieved by alternative switching. (a) Current flow and voltage for the RF turn-on phase, (b) Same for the RF turn-off phase.

In the non-oscillation phase, SW1 is open and SW2 is closed (then $V_{ak} \sim 0$ V and $I_b \sim 0$ A). This alternative double-switch operation is very important to avoid a discharge of the modulation-anode DC power supply and the capacitor. Consequently, a very sharp current rise time is realized (3 μ s). As a

result, the excitation of the competing adjacent $TE_{30,8}$ mode is suppressed. In addition, the heat loads in the cavity and collector decrease during the modulation. Therefore, operation of more than 1 MW is possible. In figure 14, an example of 60 sec, 5 kHz power modulation at 1.1 MW is shown [60].

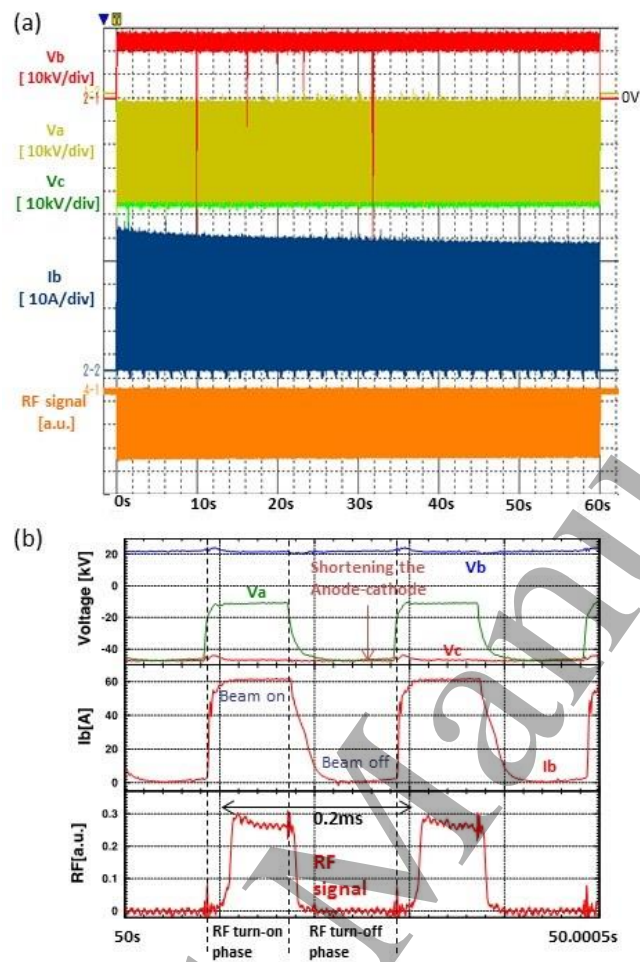


Figure 14. Experimental result of 5 kHz power modulation with full-current modulation using double modulation-anode switching [60]. (a) Signals for 60 s power modulation. (b) Zoomed signals from 50 to 50.0005 s. The pulse power is 1.1 MW.

(c) Reliability

For simulation of ITER operation, 600 s pulses of 0.8 MW were repeated with an interval of 20 ~ 30min. 72 shots of 88 trials were very stable over the full pulse duration. The other pulses were interrupted by internal arcing, etc. The operational reliability will increase by employing a fast re-start system during the pulse (Section 5.7.2). This gyrotron generated a total of 250 GJ of output energy without trouble [61,62].

(d) $TE_{31,11}$ -mode gyrotron

To increase the output power to more than 1 MW, a $TE_{31,11}$ -mode gyrotron was fabricated and tested. Its outside appearance and geometrical size are identical to the $TE_{31,8}$ -mode tube. The radius of the larger $TE_{31,11}$ -mode cavity is 20.87 mm, so that the heat load on its wall is ~1.4 times lower than that for the $TE_{31,8}$ mode. Therefore, more than 1 MW output power is available, or a larger safety margin is maintained for 1 MW operation. In addition, the $TE_{31,11}$ mode is very attractive for multi-frequency operation as described in Section 5. A concern of this higher-mode operation was the stronger mode competition. In fact, the $TE_{31,11}$ -mode oscillation is often limited by adjacent counter-rotating modes such as the $TE_{28,12}$ mode. However, reliable performance of this $TE_{31,11}$ -mode gyrotron for ITER

ECH&CD has been obtained by introducing active modulation-anode voltage and beam radius control and optimizing the electron beam position in the cavity to suppress excitation of the counter-rotating modes. Long-pulse operation of 1.0 MW with 46 % efficiency for 300 s has been achieved. 1.2 MW output power operation was achieved for up to 5 s [63]. In 2018, the first of these $TE_{31,11}$ -mode gyrotrons satisfied the ITER criteria [64].

4.1.3 Russian ITER gyrotron

The ITER gyrotron from Russia was developed by IAP, GYCOM, and the Kurchatov Institute Moscow [19,65-69]. The tube uses a diode-type MIG, a non-axisymmetric conical all-metal beam tunnel, an advanced four mirror quasi-optical output coupler and a single-stage depressed collector (top version insulator) with tapered inner diameter keeping the impact area of the spent electron beam approximately constant. Vertical electron beam sweeping (VFSS) is employed. The oscillation mode in the cavity is $TE_{25,10}$. The mini-channel cooled copper cavity has an inner radius of 17.77 mm.

(a) High efficiency long-pulse operation

Four Russian gyrotron prototypes (figure 15) were tested with CRYOMAGNETICS (USA) and JASTEC (Japan) cryogen-free SCMs. It is important to note that all gyrotrons demonstrated very similar output parameters. 1 MW output power at 1000 s pulse duration and 53-56 % overall efficiency has been achieved in single-stage depressed collector operation. For 100 s pulses, even 1.2 MW power at the same efficiency was obtained. The Gaussian output mode purity was around 97 %.

(b) Power modulation

The Factory Acceptance Test (FAT) requirements for full on/off power modulation are:

- 3 pulses 1MW/200 s ON/OFF modulated at 100 Hz
- 3 pulses 1MW/200 s ON/OFF modulated at 500 Hz
- 3 pulses 1MW/200 s ON/OFF modulated at 1000 Hz.

All tested tubes fulfilled these specifications.



Figure 15. Left: Russian 170 GHz ITER gyrotron. Right: Gyrotron together with SCM, MOU and relief load in the support structure (X-ray shielding is removed).

(c) Reliability

In 2014 gyrotron run tests at 1 MW output power with pulse durations of 500 s and 1000 s were performed. After conditioning the reliability of gyrotron operation was higher than 95 % (figure 16).

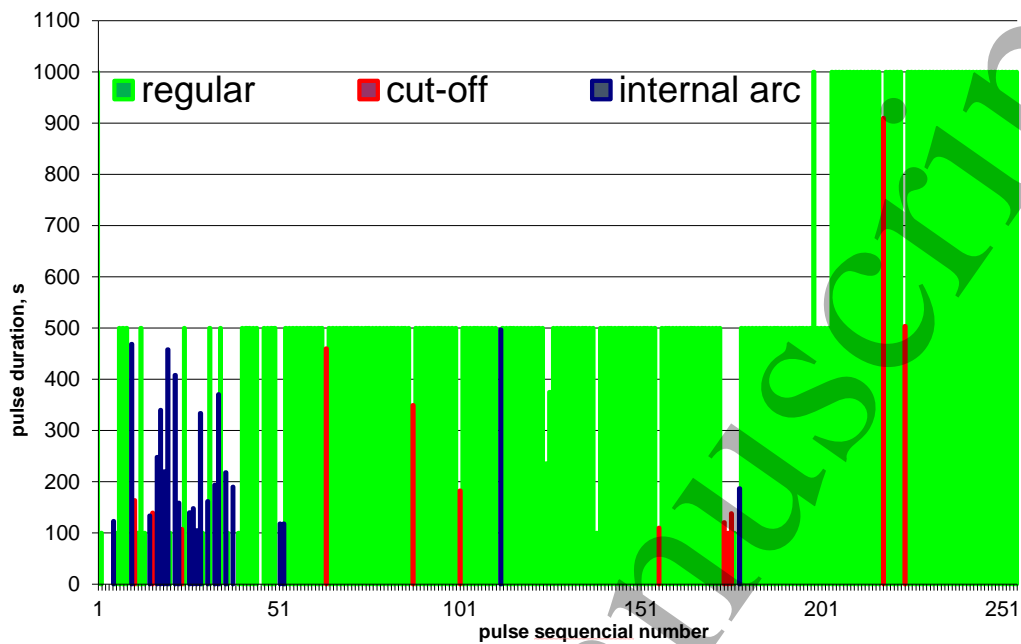


Figure 16. Gyrotron run test at 1 MW output power with pulse durations of 500 s (160 pulses) and 1000 s (55 pulses). The first 50 pulses are used as conditioning pulses.

The development of the gyrotron system for ITER is based on the solution of many very difficult scientific and engineering problems. At present, the main purpose of system modifications is to enhance system reliability and the implementation of all gyrotron systems into the ITER machine and its control and safety system. In May 2015 a prototype of the Russian ITER gyrotron system was completed and its operation was demonstrated. The system includes the gyrotron tube, cryogen-free SCM, supplementary magnets, several electric power supplies, cooling systems, control and protection systems, and other auxiliary units (figure 17).



Figure 17. Shielded gyrotron system with HE₁₁-mode waveguide, calorimetric millimeter-wave load and cooling water manifolds (gyrotron collector and load flow rates are 20 l/s and 10 l/s, respectively).

1
2
3 The gyrotron system exhibited reliable operation with the required parameters: 170 GHz frequency,
4 1 MW output power and 55% efficiency. The tests were performed in the presence of ITER IO and
5 ITER RF DA representatives. In October 2015, the Final Design Procedure for the gyrotron system was
6 successfully passed [70,71]. The procedure included preparation of several documents such as
7 descriptions, drawings, diagrams, protocols, etc, and 20 presentations with related discussions. The
8 presented materials received a positive evaluation. In 2016, fabrication of the first serial gyrotron system
9 was completed. In 2017 the second serial gyrotron system was fabricated and tested. All three ITER
10 gyrotron systems showed reliable operation in 1000-s pulses at megawatt power levels with efficiency
11 higher than 50%. The gyrotron microwave beam was fed with low losses into a 50-mm-diameter
12 corrugated HE_{11} waveguide. The measured X-ray radiation and stray microwave radiation did not
13 exceed safety levels. In 2018 the third serial system was in fabrication.
14
15

16 17 4.1.4 European ITER gyrotron

18 The European 1 MW CW, 170 GHz industrial prototype ITER gyrotron is also a conventional (hollow-
19 cavity) tube, which has been developed by the European Gyrotron Consortium (EGYC) in cooperation
20 with the industrial partner THALES, under the coordination of the European Joint Undertaking for ITER
21 and the Development of Fusion Energy (F4E). The development started in 2008, as a risk mitigation
22 action during the development of the 2 MW, 170 GHz coaxial-cavity gyrotron for ITER and was
23 completed at the end of 2015 [72]. According to the strategy, the design of the CW gyrotron is
24 completely based on a corresponding modular short-pulse (SP) prototype and the 1 MW, 140 GHz
25 gyrotron development for the stellarator W7-X (see 4.2.3). The SP prototype was built in order to
26 validate the scientific design in terms of output RF power, total efficiency and quality of the output RF
27 beam. As with the Russian ITER gyrotron, the tube uses a diode-type MIG. The beam tunnel between
28 the MIG and cavity is a conical alternating stack of BeO/SiC(60/40) ceramic damping rings and indented
29 copper rings. The cavity mode is $TE_{32,9}$. The porous-structure cooled Glidcop cavity has an inner radius
30 of 19.24 mm. In contrast to the Japanese and Russian tubes, the body insulation is located in the lower
31 part of the tube, close to the MIG (bottom type insulator, see figure 5), and the advanced three-mirror
32 q.o. output coupler has no adjustable last mirror. The collector uses 7 Hz vertical electron beam sweeping
33 combined with 50 Hz transversal sweeping with 6 coils located around a stainless steel collector section.
34 The SP prototype was successfully tested at the KIT test facility with its OXFORD INSTRUMENTS
35 superconducting magnet equipped with an additional normal-conducting coil to reach the required
36 magnetic field of 6.78 T. The scientific design of the individual tube components were verified, with the
37 gyrotron delivering an output power of 1.0 MW at 170.1 GHz with 30 % efficiency (in non-depressed
38 collector operation) and with an output RF beam Gaussian mode content of about ~ 97 % [73].
39
40

41 (a) Long-pulse operation

42 The industrial CW prototype was delivered to the KIT test facility (figure 18) in early 2016 and the
43 experiments started immediately in the short-pulse regime (with pulse lengths less than 10 ms) [74]. The
44 optimal operational parameters that were determined with short-pulses were then used as a starting point
45 for conditioning the tube with RF and slowly extending the pulse length. After approximately seven
46 weeks of conditioning, it was possible to operate the gyrotron with more than 0.8 MW output power at
47 pulse lengths up to 180 s, which is the limit at the High-Voltage (HV) power supply that is currently
48 available at KIT. Up to that point, the maximum efficiency was 38 % (in depressed collector operation)
49 with a Gaussian mode content of the output RF beam of at least 97 % [75,76]. The reason for the reduced
50 power performance of the industrial CW prototype is not known up to now. For further investigation
51 and pulse duration extension up to one hour, the CW prototype was delivered to the Swiss Plasma Center
52 (SPC), Lausanne, where the tube will be operated with the designated SCM manufactured by
53 CRYOGENICS (figure 19). Power modulation and reliability of the tube will also be investigated.
54
55
56
57
58
59
60

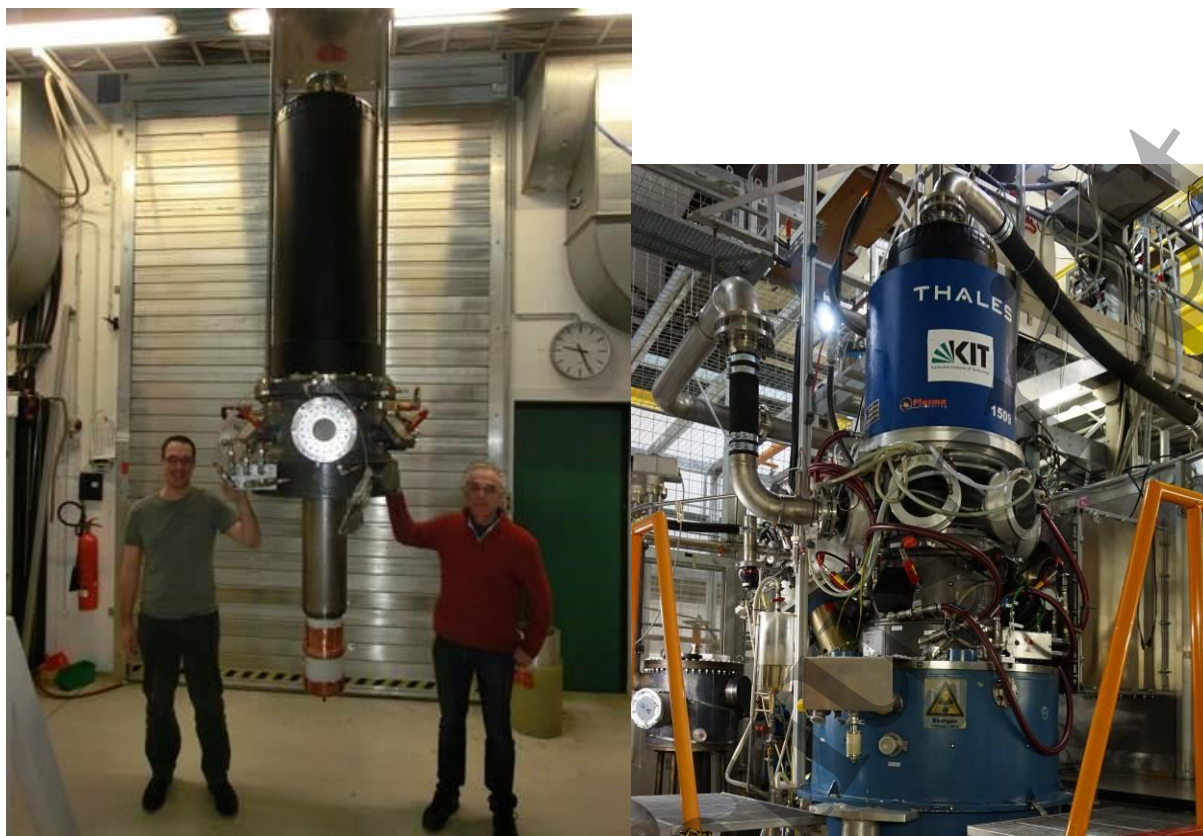


Figure 18. The EU 1MW, 170 GHz CW industrial prototype gyrotron (left) installed in the KIT OXFORD INSTRUMENTS superconducting magnet (right) (© 2017 IEEE. Reprinted, with permission from [76] Ioannidis ZC et al 2017, IEEE Trans. on Electron Devices 64, 9, 3885).



Figure 19. The EU 1MW, 170 GHz CW industrial prototype gyrotron installed at SPC with the CRYOGENICS superconducting magnet. The gyrotron is connected to the calorimetric RF load [50] using an MOU and an HE₁₁-mode waveguide under vacuum.

4.1.5 Comparison of the different ITER gyrotrons

The design parameters, specifications and typical results of the different 170 GHz ITER gyrotrons are summarized in table 1.

Table 1. Parameters and typical results (up to the end of 2018) of the Japanese and Russian 170 GHz ITER gyrotrons and of the first European prototype tube developed for ITER.

	JA	RF	EU
Operating Cavity Mode	TE31,8 / TE31,11	TE25,10	TE32,9
Radial Mode Eigenvalue	63.76750 / 74.32574	63.31966	68.56314
Cavity Radius	17.9 mm / 20.87 mm	17.77 mm	19.24 mm
Electron Beam Radius	9.13 mm	7.4 mm	9.5 mm
Launcher Angle	0.2 deg.	0.2 deg.	0.23 deg.
Output Mode Purity	96 %	97 %	97 %
Output Power	1 MW (0.8 MW) / 1 MW (1.2 MW)	1 MW (1.2 MW)	0.8 MW
Pulse Duration	800 s (3600 s) / 300 s (2 s)	1000 s (100 s)	180 s
Overall Efficiency	55 % (57 %) / 46 % (47 %)	54 % (53 %)	38%
Magnetron Injection Gun	Triode	Diode	Diode
Electron Beam Energy	72 keV	70 keV	72 keV
Depression Voltage	30 kV	27.5 kV	25 kV
Beam Current	43 A	42 A	45 A
Mean Emitter Radius	46.5 mm	41.5 mm	53.5 mm
Magnet Bore Hole	240 mm	160 mm	220 mm

4.2 Gyrotrons for the long-pulse plasma experiments LHD, QUEST, JT-60SA, EAST, KSTAR, W7-X, and Tore Supra

4.2.1 Japanese gyrotrons for LHD, QUEST, and JT-60SA

The ECH system of JT-60U using 110 GHz gyrotrons stopped its operation in 2008. Its performance has been summarized in [81]. Now JT-60U is being upgraded to JT-60SA, which is a joint international R&D project involving Japan and Europe using the existing infrastructure of JT-60U. A gyrotron enabling high-power, long-pulse operation at both 110 GHz and 138 GHz has been developed for ECH&CD in JT-60SA. The configuration of the JT-60 SA EC system is shown in figure 20. Operation at 1 MW for 100 s has been demonstrated at both frequencies in 2014 [82]. After this, high-power gyrotron development toward 1.5 – 2 MW output power for several seconds was carried out. In 2015, stable oscillation of 1.5 MW for 5-s pulses was demonstrated as a first step to confirm the high-power capability in comparison with previous gyrotron version. Operation at even higher power has been carried out toward a goal of 2 MW, which is the maximum acceptable power for the cavity in design. An oscillation of 1.9 MW for 1-s pulses has been obtained. However, mode competition with the adjacent modes or counter-rotating modes at pulse lengths from 0.1 s to 0.5 s limits the pulse length at power levels higher than 1.9 MW, so far. The rise time of the power supply is approximately 0.1 s. Thus a

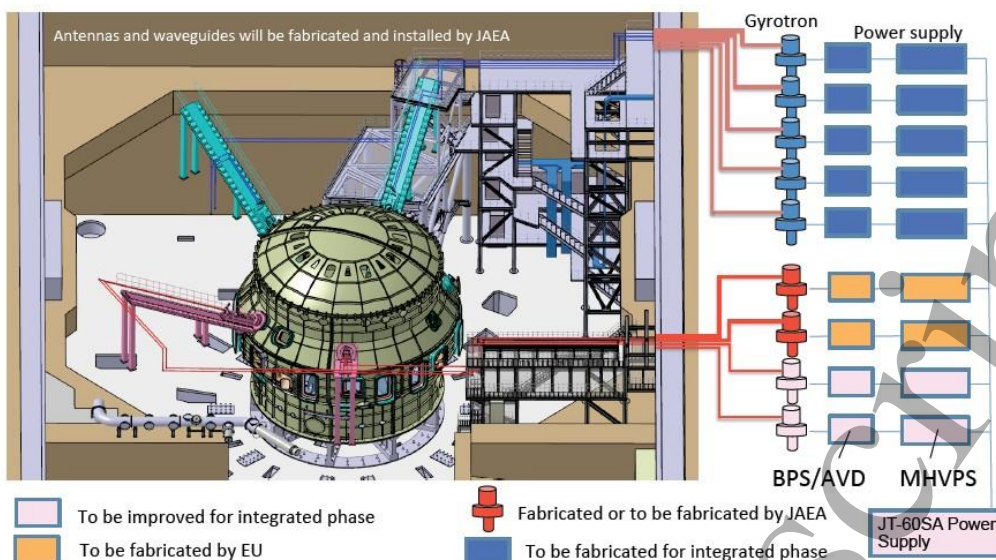


Figure 20. Conceptual view of the JT-60SA and its ECH&CD system. A power injection of 3 MW with 4 gyrotrons is planned in the initial stage, and will be upgraded to 7 MW power using 9 gyrotrons in the final stage (integrated phase). JAEA was renamed as QST.

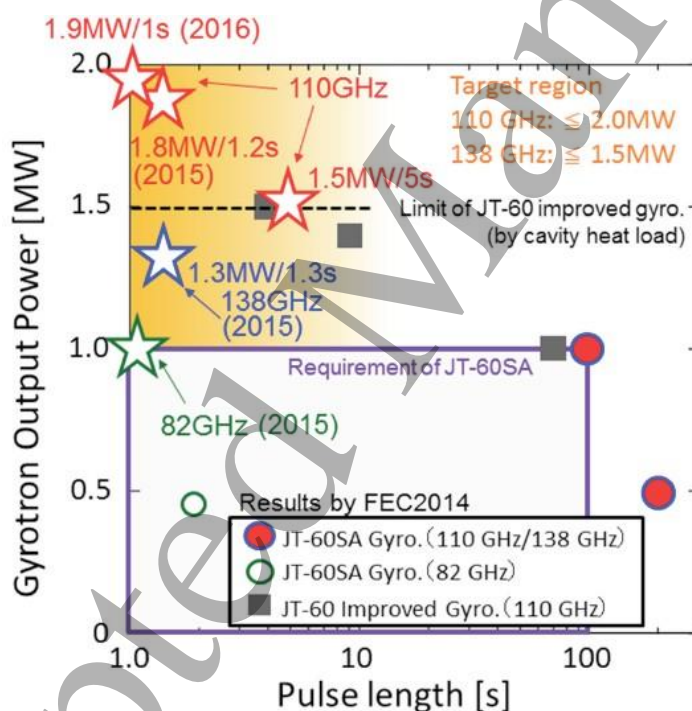


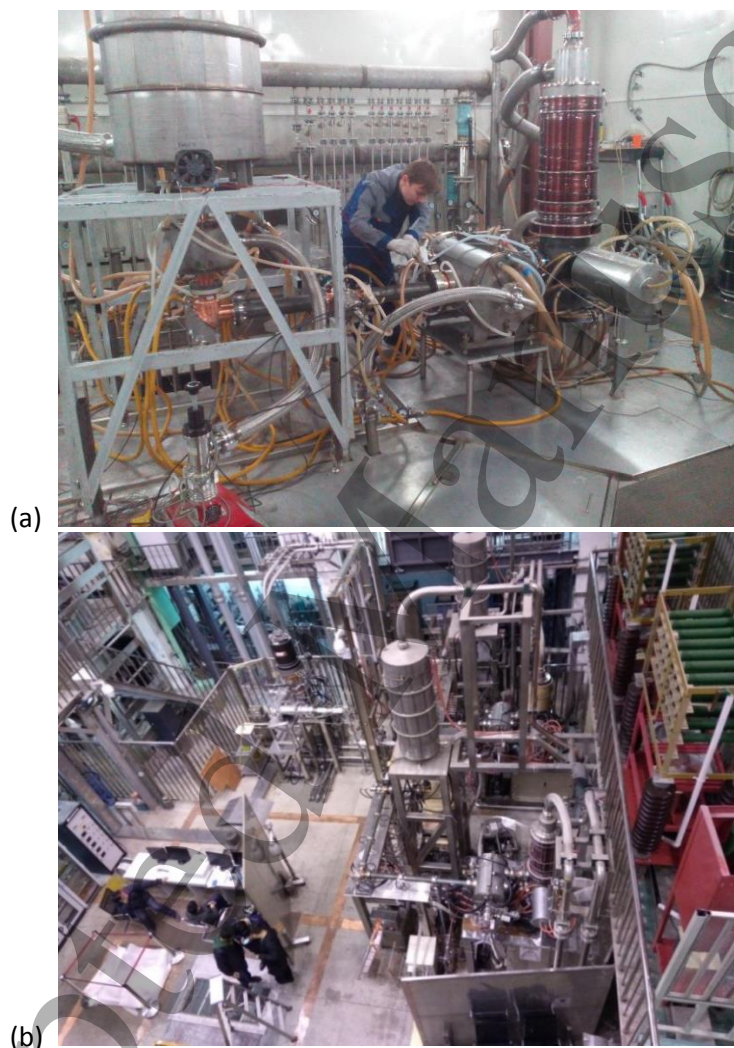
Figure 21. Status of gyrotron performance for JT-60SA.

change in the oscillation condition, which results in mode competition, appeared after the applied voltages reached flat top values. In addition to the above result at 110 GHz ($TE_{22,8}$ -cavity mode), oscillations of 1.3 MW for 1.3-s pulse duration at 138 GHz ($TE_{27,10}$ mode) and 1 MW for 1-s pulses at 82 GHz ($TE_{17,6}$ mode) have been demonstrated. The achieved power and pulse length at each frequency is summarized in figure 21 (see also Section 5.3.2).

4.2.2 Russian gyrotrons for EAST and KSTAR

GYCOM in collaboration with IAP designed, manufactured and tested a series of long-pulse gyrotrons in the 105-140 GHz frequency range with parameters similar to the ITER tubes [19,46,67,68,83]. Two-

1
2
3 frequency 140/105 GHz 1 MW TE_{22,8}/TE_{17,6}-mode gyrotrons with 1.8 mm thick plane CVD-diamond
4 window disks operating with a pulse duration of 300 s were successfully tested at the customer site at
5 NFRI in Korea. The overall gyrotron efficiency calculated by taking into account the TEM₀₀-mode
6 content in the output power, reached 50-55 %. At present time this gyrotron operates at the plasma
7 machine KSTAR in Korea. The second tube of this type has been delivered to NFRI. Development of
8 these two-frequency gyrotrons required solving several key tasks, as effective excitation of the two
9 operating cavity modes, design of the q.o. mode converter that transforms the different cavity modes at
10 different frequencies into a Gaussian output wave beam, and the design of a gyrotron collector that
11 is consistent with the various guiding magnetic fields. Since the TE_{22,8}-cavity mode at 140 GHz is co-
12 rotating and the TE_{17,6} mode at 105 GHz is counter-rotating, the magnetic field has to be reversed for
13 proper performance of the q.o. output coupler.
14



49 **Figure 22.** 140 GHz gyrotron setup for EAST tokamak during factory test (a), two GYCOM gyrotrons
50 with MOU, waveguides and terminal loads installed at EAST site (b) (photo in April, 2018). Upper
51 photo shows the system installed in 2015, lower photo corresponds to the system accepted in 2018.
52

53 A GYCOM/IAP 140 GHz, 1 MW, 1000-s gyrotron has operated at the EAST tokamak at ASIPP in
54 China since the middle of 2015. The second tube of this gyrotron type passed the factory tests in July
55 2016, and the acceptance tests at the beginning of 2018. Figure 22 shows one of the tubes at the factory
56 tests and the same tube installed at the ASIPP site. Beside the gyrotrons, all of the deliveries to KSTAR
57 and EAST include other components of the gyrotron complex, including superconducting magnets
58 (produced by JASTEC, Japan), MOUs, elements for the evacuated HE₁₁ transmission lines and full-
59 power evacuated dummy loads.
60

4.2.3 European and US gyrotrons for W7-X and EU Tore Supra gyrotron

Megawatt-class 140 GHz long-pulse gyrotrons with 1.80 mm thick CVD diamond output window and single-stage depressed collector were developed by CPI and the EU team (KIT, SPC, THALES, Max Planck Institute for Plasma Physics in Greifswald (IPP Greifswald), IPF University of Stuttgart), independently, for the 10 MW ECH&CD system of the W7-X stellarator at IPP Greifswald. The specifications are listed in table 2. Both gyrotrons have been successfully tested for CW operation using the power supply of IPP [84]. The ECH&CD system of W7-X is routinely operated employing nine THALES gyrotrons and one CPI tube.

-CPI gyrotron [84,85]

A photo of the CPI gyrotron is shown in figure 23 (a). The tube has a diode-type MIG. The body voltage is supplied from a second terminal from the bottom (bottom version insulator). The collector is grounded and the -55 kV cathode voltage is supplied from the bottom terminal. After the test at CPI, where 500 kW with 600 s was obtained for numerous shots, the tube was sent to IPP Greifswald. 0.9 MW power output was demonstrated for 30 min for the first time in 2005. The efficiency was ~ 36 % with +25 kV body voltage. The measured internal diffraction loss is 4% of the generated power. Two of these megawatt-class 140 GHz, CW CPI gyrotrons are being used at EAST at ASIPP in Hefei, China [86].

Table 2. Specification and typical results of 140-GHz gyrotrons of EU and United States (CPI) developed for W7-X.

	EU	US
Frequency	140 GHz	140 GHz
Cavity Radius	20.48 mm	19.26 mm
Cavity Length	14.5 mm (straight)	16.46 mm (straight)
Electron Beam Radius	10.1 mm	10.1 mm
Diffraction Q-Factor	1100	1200
Cavity Mode	TE _{28,8}	TE _{28,7}
Output Mode Purity	98.0 %	97.5 %
Launcher Angle	0.229 deg.	0.14 deg.
Output Power	1.0 MW	1.0 MW
Pulse Duration	1800 s (CW)	1800 s (CW)
Overall Efficiency	48 %	42 %
Magnetron Injection Gun	Diode	Diode
Electron Beam Energy	81 keV	80 keV
Beam Current	40 A	40 A
Depression Voltage	27-30 kV	20 kV
Experimental Results	0.92 MW/1800 s/44 %	0.9 MW/1800 s/36 %
	1.02 MW/360 s/43 %	

-EU gyrotron [19,34,84,87-90]

A photo of the EU gyrotron is shown in figure 23 (b). The tube also has a diode-type MIG and bottom version insulation of the depression voltage. The collector uses 7 Hz vertical electron beam sweeping combined with 50 Hz transversal sweeping. The measured inner stray radiation loss only amounts to ~ 2% due to the high efficiency internal mode converter [91]. At IPP an output power of 0.92 MW in 30 min. operation was obtained. The efficiency was 44% using an SDC. Very high efficiency q.o. mm-wave transmission of approximately 90% was measured for a 25 m long line with 17 mirrors [30]. The series production of seven tubes was done at THALES. Together with the corresponding two THALES prototype gyrotrons, nine THALES tubes are in operation at W7-X, as already mentioned above [7]. The power-modulation capabilities of the THALES tube have also been experimentally investigated. Modulation depths higher than 80% have been obtained either by modulating the cathode voltage or the depression voltage. Modulation frequencies as high as 50 kHz have been obtained with cathode voltage modulation and 1.5 kHz with depression voltage modulation [92].



Figure 23. The 140-GHz gyrotrons for W7-X [19] developed by (a) the US (CPI) and (b) the EU team.

A 0.5 MW, 118 GHz long-pulse gyrotron (without SDC) with a q.o. output coupler and a cryogenically cooled single-disk sapphire output window was developed by the EU team in collaboration with THALES for Tore Supra and TCV [87,93]. It operates in the $TE_{22,6}$ -cavity mode and delivers 0.53 MW in 5-s pulses and 0.35 MW in pulses with 111-s duration.

4.3 Gyrotrons for moderate pulse-length plasma devices (GAMMA 10, DIII-D, AUG, TCV, HL-2A)

4.3.1 Japanese gyrotrons for GAMMA 10

As already mentioned in Section 4.2.1, megawatt-class 28 GHz fusion gyrotrons with a q.o. output coupler and SDC for the mirror machine GAMMA 10 are under development in Japan in collaboration with Tsukuba University, QST, NIFS and CETD. The operating cavity mode is $TE_{8,3}$. The maximum output power obtained is 1.38 MW, which is a new record at this frequency. In long-pulse operation, 0.6 MW for 2 s at 28 GHz has been achieved [79]. For the next step of the 28 GHz gyrotron development, the test of a gyrotron with greater than 1.5 MW output power has begun to study multi-MW oscillation. The possibility of 0.4 MW CW and 2 MW output power for pulse durations of a few seconds, after improvements to the output window and mode converter, is being investigated. This gyrotron can oscillate at two frequencies, 28 and 35 GHz, which shows the versatility of such multi-purpose gyrotrons. In short pulses, maximum powers of 1.65 MW at 28.04 GHz and 1.21 MW at 34.83 GHz were achieved [82].

4.3.2 Russian gyrotrons for AUG and HL-2A

A 10-s pulse duration, two-frequency gyrotron was developed by IAP/GYCOM in Russia for use in the ECH&CD system on ASDEX Upgrade at IPP Garching (see 4.2.2) [94]. Currently, eight tubes are running there. By changing the magnitude and direction of the magnetic field in the cavity, the operating mode is controlled. The generated powers and frequencies are 0.85 MW and 0.95 MW for 105 GHz and 140 GHz, respectively. The operating modes are $TE_{17,6}$ and $TE_{22,8}$ at 105 GHz and 140 GHz, respectively. The results show that the q.o. mode converter works well for both frequencies/modes. This is the first two-frequency gyrotron that has ever been used in an ECH&CD experiment. The transmission loss in the corrugated HE_{11} mode transmission line to the tokamak is low, i.e., 12% and 10% at 105 GHz and 140 GHz, respectively. Two corresponding megawatt-class 140 GHz gyrotrons with 3 s pulse duration are in operation at the HL-2A tokamak in Chengdu, P.R. China.

4.3.3 European gyrotrons for TCV

Three 2 s pulse duration versions of the 0.5 MW, 118 GHz gyrotron developed by the EU team in collaboration with THALES for Tore Supra (see 4.2.3) are in operation at TCV [87,93]. In one of these tubes the cryogenically-cooled sapphire window was replaced by a water cooled 1.6-mm-thick CVD-diamond window. Currently, an upgrade of the EC-system for the TCV tokamak has begun and is part of a broader upgrade of TCV [95].

Table 3. Dual-Frequency Gyrotron Design Parameters.

Operating Cavity Mode	TE _{17,5}	TE _{26,7}
Frequency	83.91 GHz	126.16 GHz
Output Power	1.05 MW	1.2 MW
Cavity Wall-Loading	1.1 kW/cm ²	2.1 kW/cm ²
Electron Beam Current	40 A	40 A
Electron Beam Energy	78 keV	78 keV
Modulation-Anode Voltage	-38 kV	-26 kV
Electron Pitch Factor	1.3	1.3
Cavity Magnetic Field	3.31 T	4.98 T
Electronic Efficiency	35 %	41 %
Gaussian Mode Content	97.7 %	97.6 %

A MW-class dual-frequency gyrotron (84 or 126 GHz, 2-s pulse duration, 1 MW power level) has been developed by the EU gyrotron team [95]. The design parameters are listed in table 3. Two tubes are being manufactured by THALES. The first gyrotron was already installed at the TCV site and successfully tested at short pulses (10 ms). It delivers 0.9 MW and 1.0 MW at the lower and higher frequencies, respectively, in a high-purity Gaussian output beam [96].

4.3.4 US gyrotrons for DIII-D

For higher performance of the CPI 110 GHz gyrotrons [97-100], a project for 1.5 MW gyrotron output power is underway in the USA. As a physics research project, a 110 GHz, high efficiency 1.5 MW gyrotron with 48% overall efficiency was operated at MIT in short pulses (3 μ s). The cavity was carefully designed taking into account the probable competing modes [101]. The operating cavity mode is TE_{22,6}. The tube contains a built-in q.o. output coupler and a depressed collector. Parallel to this development a corresponding long pulse 110 GHz gyrotron and a 117.5 GHz tube (TE_{20,9}) is on-going at CPI. Up to now, short pulse operation at 1.28 MW output power with 42.3% efficiency and 1.7 MW at 37 % efficiency was obtained at 110 GHz and 117.5 GHz, respectively [102,103]. Long-pulse operation aiming at 1.3 MW is being carried out at General Atomics. Up to now the 117.5 GHz gyrotron has achieved 1 MW for 5 s.

5. Development of future advanced fusion gyrotrons

5.1 Higher gyrotron frequencies for DEMO

The ECH&CD system of a future, commercially attractive tokamak DEMONstration fusion reactor operating under stationary conditions must be optimized to provide maximum possible CD efficiency. The achievable ECCD efficiency in two DEMO scenarios has been investigated in [6], one for pulsed- and one for steady-state operation. Millimeter (mm)-wave beam propagation, absorption and current drive have been simulated employing beam-tracing techniques and including momentum conservation in electron-electron collisions. For mid-plane wave launching the achievable CD efficiency has been found to be limited by 2nd-harmonic absorption. Higher efficiencies can be obtained by injecting the millimeter (mm)-wave beams from the top of the tokamak, using wave absorption by more energetic, less collisional electrons and due to the reduced number of trapped electrons that absorb the waves. CD efficiencies competitive with those usually achieved by neutral beam CD have been calculated.

Assuming the EUROfusion 2012 baseline for DEMO with an aspect ratio $A = R/a$ (major/minor plasma radius) of 4.0 and $B > 7$ T the operation frequencies for optimum ECCD are significantly above 200 GHz, while lower frequencies around 170 GHz and 200 GHz appear useful for plasma start-up and bulk heating. However, in the meantime DEMO machines with smaller aspect ratio are being discussed [13]. Table 4 summarizes the gyrotron frequencies, f , required for ECH and ECCD as a function of aspect ratio and magnetic field. Even for $A = 3.1$ frequencies of up to approximately 200 GHz are needed.

Table 4. Gyrotron frequencies f needed for plasma heating and current drive for different values of the aspect ratio A and toroidal magnetic field B_t (γ is a measure of the current drive efficiency).

$A = R/a$	2.60	3.1	3.6	4.0
B_t	4.2 T	5.7 T	7.0 T	7.6 T
f for Heating	118 GHz	160 GHz	197 GHz	213 GHz
f for Current Drive	144 GHz	196 GHz	240 GHz	280 GHz
γ (Top Launch)	0.16 A/m ² MW	0.32 A/m ² MW	0.36 A/m ² MW	0.45 A/m ² MW

The requirements for DEMO gyrotrons are as follows: 2 MW unit power, > 95 % Gaussian output beam purity, > 60 % overall efficiency, > 99 % reliability, multi-frequency capability for different functions of the ECH&CD system, and if possible, fast (within a few seconds) step-wise frequency tunability in 2-3 GHz steps within the maximum frequency span of ± 10 GHz for plasma stabilization employing simple fixed antenna systems [104]. Such tubes need broadband or tunable CVD-diamond output windows [19,40-42,67,105-107]. The development of electron guns with high beam quality and of multi-stage depressed collectors (MSDC) for energy recovery is necessary to achieve such a high efficiency.

5.1.1 Japanese developments for future DEMO gyrotrons

Two activities relevant to DEMO gyrotrons have been carried out in Japan. First, the Japanese multi-frequency gyrotron was operated at 203 GHz and 7.98 T cavity magnetic field. This successful result is discussed in Section 5.3.2. The second activity is basic research using a short pulse test, sub-THz gyrotron, which was developed by QST (JAEA) and shown in figure 24. The gyrotron employs a 13-T SCM with a 110-mm warm-bore diameter, also designed at QST (JAEA) [79]. The cavity is designed to generate a maximum frequency of 300 GHz in the $TE_{32,18}$ mode. The power is extracted via an axial output/collector waveguide without a q.o. mode converter. The experiment was carried out at University of Tsukuba, in collaboration with QST. More than 0.6 MW output power was measured in 2-ms pulses at 20 % efficiency, as shown in figure 25 [108]. The highest output power was achieved by inclining the output window disk by 1.15 deg. (black circles) to avoid mode trapping inside the tube. By decreasing the magnetic field, oscillation of lower frequencies around 240 GHz was demonstrated by scanning the cavity magnetic field. Up to now, 345 kW was obtained at 243.9 GHz ($TE_{28,14}$) [79].

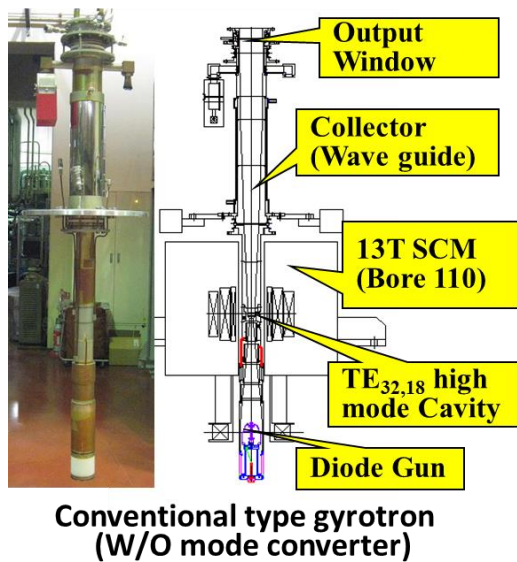


Figure 24. QST 300 GHz gyrotron

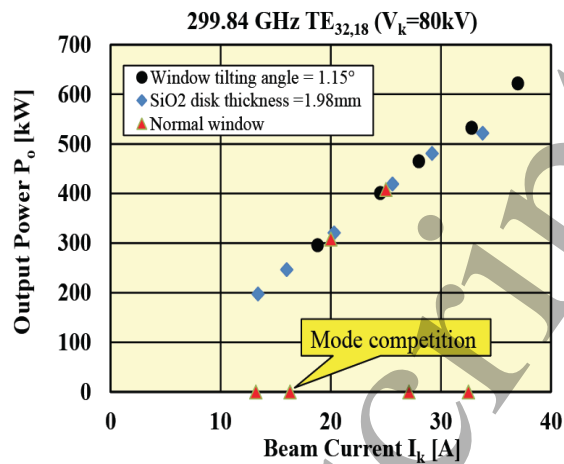


Figure 25. Output power vs. electron beam current for the QST 300 GHz gyrotron.

5.1.2 Russian developments for future DEMO gyrotrons

At the IAP, in collaboration with GYCOM, a prototype fundamental frequency 250 GHz gyrotron for 200 kW CW operation was designed and tested (see figure 26) [109,110]. For this tube a magnetic field of more than 9.5 T is required, which is available in the cryogen-free JASTEC SCM (JM10T100) at the IAP, with a 100-mm warm-bore diameter. This warm-bore diameter determined the dimensions of the electron optics and cavity, taking into account the technical requirements for cooling systems. As a result, to ensure stable RF generation at the selected frequency, the $TE_{19,8}$ mode was selected as the working mode with a cavity radius of 9.34 mm. Due to the close coupling factors of this operating cavity mode and the parasitic modes $TE_{18,8}$ and $TE_{20,8}$, the optimal radius of the electron beam in the interaction cavity is $R_{\text{beam}} = 3.93$ mm, which differs slightly from the radius of maximum coupling coefficient for the working mode $R_{\text{opt}} = 3.85$ mm. The length of the homogeneous cavity section was chosen to be $L = 10$ mm. The calculated operational parameters of the gyrotron are summarized in table 5.



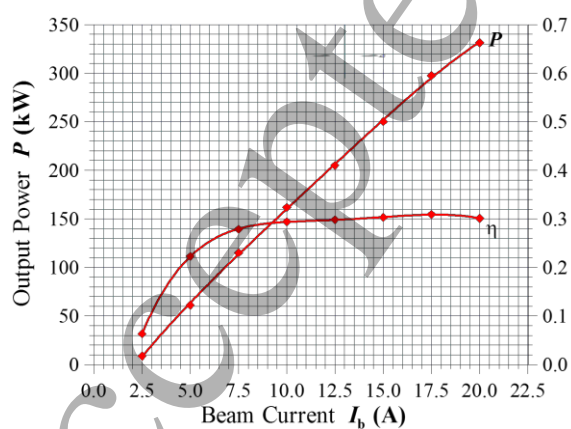
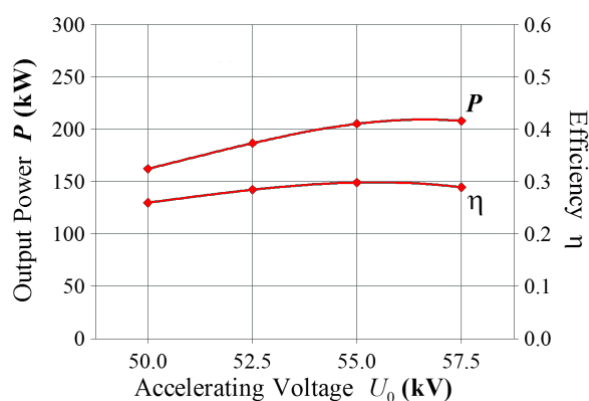
Figure 26. Photo of the IAP/GYCOM 250 GHz, 200 kW, CW gyrotron in the 10 T JASTEC SCM.

Table 5. Design parameters of the IAP/GYCOM 250 GHz, 200 kW, CW gyrotron.

Operating Frequency	250 GHz
Operating Mode	TE _{19,8}
Cyclotron Harmonic	1
Accelerating Voltage	55 kV
Depressed Collector Potential	30 kV
Cavity Magnetic Field	9.6-9.7 T
Beam Current (nominal in CW mode)	12 A
Beam Current (pulsed mode)	20 A
Cavity Radius	9.34 mm
Cavity Length (homogeneous part)	10 mm
Beam Radius inside Cavity	3.93 mm
Pitch Factor	≥ 1.1

The tube is equipped with an internal q.o. wave beam converter, which transforms the cavity mode into a Gaussian TEM₀₀ beam and couples it radially to the output vacuum window. The converter consists of a shaped waveguide, a curved mirror, four flat mirrors, and a synthesized mirror with a non-quadratic curvature function.

The first experimental tests were carried out at the IAP RAS. Due to the limitations of the HV power supply, the first experiments were carried out in short pulses. For these tests a removable BN output window with 66 mm aperture diameter was manufactured and installed. The thickness of the window was chosen to be about 3.1 mm in order to minimize reflections at the operating frequency of 250 GHz. The pulse duration in the experiment was 20-40 μ s with a repetition frequency of 10 Hz. The frequency of the output radiation was measured using a resonant-cavity wavemeter. 249.74 GHz operation at 200 kW was obtained at the following parameters: 55 kV accelerating (cathode) voltage, 12.5 A electron beam current, and 9.625 T magnetic field. These results agree with the simulation data. A reduction of the thermal load in the cavity during pulsed operation made it possible to test the gyrotron with parameters exceeding the nominal design values. Thus, with an increase of the beam current to 20 A, it was possible to reach a power of 330 kW at an accelerating voltage of 55 kV. The obtained experimental results are shown in figures 27 and 28. Measurements of the transverse intensity distribution of the mm-wave beam formed by the built-in q.o. mode converter were made, and the content of the TEM₀₀ Gaussian beam wave was estimated. The measurement was performed using the thermal imaging technique [36] in several cross sections along the propagation of the wave beam. The analysis showed a Gaussian mode content in the reconstructed wave beam of 98.6%.

**Figure 27.** Output power and efficiency vs. electron beam current at $V_b = 55$ kV for the IAP 250 GHz gyrotron.**Figure 28.** Output power and efficiency vs. acceleration voltage at $I_b = 12.5$ A for the IAP 250 GHz gyrotron.

5.1.3 EU developments for future DEMO gyrotrons

Within the Work Package Heating and Current Drive (WPHCD), coordinated by the Power Plant Physics and Technology Department of EUROfusion, detailed studies are ongoing, which cover three different systems for plasma heating and current drive. These are, namely, systems using electron cyclotron waves, ion cyclotron waves, and neutral beam injection. The studies are in line with the European Fusion Roadmap towards a DEMO [13,111]. Following the development of 1 MW, CW 140 GHz and 170 GHz gyrotrons for the W7-X stellarator and the ITER tokamak, respectively, the conceptual designs of tubes with frequencies up to approximately 240 GHz were performed at KIT-IHM [112-117]. Along with a 237.5 GHz, 2 MW coaxial-cavity gyrotron design, a 236 GHz, 1 MW hollow-cavity approach was under investigation, as backup solution. In both cases, operating modes have been selected considering multi-frequency operation at around 170 GHz/204 GHz/237 GHz and 270 GHz for multi-purpose applications and fast-frequency tunability in steps of 2-3 GHz within the frequency range of ± 10 GHz around the operating center frequency for plasma stability control.

At 237.5 GHz, a coaxial-cavity design for the $TE_{49,29}$ -mode (eigenvalue $\chi_{m,n} \sim 158$) has been found and optimized using realistic electron beam parameters with quite promising 1.9 MW output power and 33 % interaction efficiency at a maximum cavity wall loading of 2 kW/cm². At 203.8 GHz, oscillating in the $TE_{42,25}$ -mode ($\chi_{m,n} \sim 136$), the same cavity could deliver 1.9 MW output power with 32 % interaction efficiency at reduced maximum cavity wall loading of 1.7 kW/cm². For 170.0 GHz operation in the $TE_{35,21}$ -mode ($\chi_{m,n} \sim 113$), the corresponding parameters would be 1.8 MW, 31 % and 1.3 kW/cm².

In the case of a $TE_{43,15}$ -mode ($\chi_{m,n} \sim 103$) hollow-cavity gyrotron operating at 236.1 GHz (see Section 5.3.2), again considering realistic electron beam parameters in the cavity (rms velocity spread: 6 %, radial beam width: $\lambda/4$) and a realistic conductivity of the anticipated cavity material Glidcop, the results suggest stable output power of 0.92 MW with an interaction efficiency of 36 % at a maximum cavity wall loading of 2 kW/cm². For the $TE_{37,13}$ -mode ($\chi_{m,n} \sim 89$) at 203.0 GHz and the $TE_{31,11}$ -mode ($\chi_{m,n} \sim 74$) at 170.0 GHz the corresponding parameters are 1.15 MW and 1.55 MW and 35 % and 33 %, respectively.

Currently, the existing 170 GHz, 2 MW coaxial-cavity design is studied regarding multi-frequency operation. Possible operation at 170 GHz, 204 GHz and 238 GHz (window resonances) is targeted [118]. The aim of the study is to check if the actual working gyrotron can operate at the above mentioned frequencies without huge efforts in redesigning new components. The condition for mode selection is given by a maximal deviation of < 3.6 % in caustic radius compared to the one for the $TE_{34,19}$ mode. This is the condition that determines whether the quasi-optical system can perform equally well at the different frequencies. The chosen operating modes, based on using the nominal $TE_{34,19}$ -mode at 170 GHz, are $TE_{40,23}$ at 204 GHz, $TE_{48,26}$ at 237 GHz, and $TE_{46,27}$ at 238 GHz. Instrumental to the gyrotron R&D is the new Fusion Long Pulse Gyrotron Lab (FULGOR) at KIT-IHM, a test stand that is able to support the development of CW gyrotrons with a power of up to 4 MW at frequencies up to 240 GHz [119].

5.2 Sub-THz gyrotrons for Collective Thomson Scattering

Collective Thomson Scattering (CTS) diagnostics enables measurement of the ion velocity distribution function in fusion plasmas. Up to now, only gyrotrons developed for plasma heating have been used. However, high-density plasmas require very-high-frequency gyrotrons in order to avoid refraction and/or absorption. Such gyrotrons are being developed at the Research Center for Development of Far-Infrared Region of the University of Fukui (FIR-FU) in Japan. Recently, they have succeeded in achieving 83 kW at 389 GHz and 3-ms pulse duration [120]. Second harmonic oscillation was used to relax the requirements for the superconducting magnet. However, mode competition with fundamental harmonic modes has prevented operation at higher power [121]. Currently, the FIR-FU team is investigating a fundamental frequency mm-wave gyrotron for CTS, which is mounted in a cryogen-free 12 T magnet. In a first stage, the cavity mode was the co-rotating $TE_{14,2}$ mode oscillating at 295 GHz. The maximum power was 220 kW at 60 kV beam voltage, 14 A beam current and 5- μ s pulse length. The efficiency was about 25%, nearly independent of the beam current [121]. In a second stage, the

tube is now operated in the TE_{22,2} mode at 303 GHz and delivers 320 kW Gaussian-mode output power at 32.8 % efficiency and 100- μ s pulse length. The experimental results are shown in figure 29 [122].

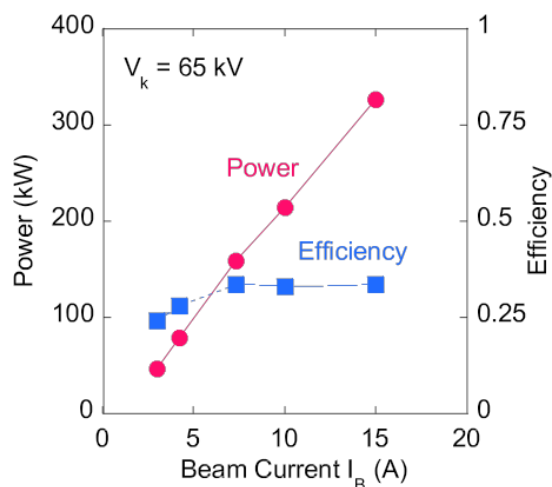


Figure 29. Measured output power (closed circles) and efficiency (closed squares) of a 303 GHz CTS gyrotron vs. electron beam current (Reprint from [122] Saito T et al 2017, Plasma and Fusion Res. Rapid Communications 12, 1206013, with permission from JSPF).

A fundamental frequency 670 GHz gyrotron with record power (210 kW) and efficiency (20%) has been developed in joint experiments of the IAP Nizhny Novgorod, Russia, and the University of Maryland in the USA [123]. The required magnetic field of 27-28 T is produced by a pulsed solenoid with several ms pulse duration. The gyrotron operates in the TE_{31,8} cavity mode and is equipped with an external q.o. mode converter. The RF-pulse duration was 20-30 μ s.

A record frequency stability was demonstrated using a 263 GHz, 100 W sub-THz gyrotron employing a phase-locked loop in the modulation-anode voltage control. The relative width of the frequency spectrum and the frequency stability were 4×10^{-12} and 10^{-10} , respectively [124]. Of course, in a long-pulse megawatt-class CTS gyrotron, sufficient frequency stabilization only may be achieved after the cavity deformation is in equilibrium.

5.3 Multi-frequency gyrotrons

The transmission frequencies of a simple, standard single-disk window are given by eq. (9). For example, the thickness of a synthetic diamond 170 GHz gyrotron window disk is $d = 1.852$ mm, corresponding to $n = 5$ half-wavelengths in CVD diamond (see Section 4). Other transparent frequencies are 102, 136, 204 and 238 GHz. If one finds for a cavity with radius R_{cav} a series of modes with the same sense of rotation, oscillating very close to these window transmission frequencies and having very similar caustic radii $R_c = (m/\chi_{m,n}) R_{cav}$, the gyrotron can be operated as a multi-frequency (multi-purpose) gyrotron just by selecting the correct electron beam position and setting the proper external magnetic field in the cavity as discussed in Section 2. Since the Brillouin angles $\theta_B = \arccos[1 - (R_{cav}/R_L)^2]^{1/2}$ in the launcher of the q.o. output coupler with radius R_L , the azimuthal radiation spread angles at the launcher aperture $2\phi = 2\arccos(m/\chi_{m,n})$ and the required launcher cut length $L = 2\pi R_L \sin\phi / (\phi \tan\theta_B)$ for the various modes are also almost the same, the q.o. output coupler can provide a Gaussian output beam for this series of modes at different frequencies [113]. Of course, the wave beams have to be matched to the transmission line by specific correction mirrors in a matching optics unit (MOU).

5.3.1 Two-frequency gyrotrons in Russia and EU

A two-frequency gyrotron is technically the simplest variant of a multi-frequency gyrotron. Two-frequency 140/105 GHz 1 MW TE_{22,8}/TE_{17,6}-mode GYCOM gyrotrons with 1.8 mm thick CVD-diamond window disks operating with pulse duration of up to 300 s are successfully operated at ASDEX Upgrade in Germany, KSTAR in Korea and HL-2A tokamak in Chengdu, P.R. China (see Section 4).

The ASDEX Upgrade tubes with 10-s pulse duration were the first two-frequency gyrotrons to be used in an ECH&CD experiment [94]. The generated powers and frequencies are 0.85 MW and 0.95 MW at 105 GHz and 140 GHz, respectively. To obtain the maximum transmission line efficiency for both frequencies, the two MOU mirror sets are mounted on a revolving support for exchange when the frequency is changed. The measured transmission loss in the corrugated HE₁₁-mode transmission line to the tokamak is low, i.e., 12% and 10% at 105 GHz and 140 GHz, respectively.

For future multi-purpose applications, the Russian 170 GHz, 1 MW, 1000 s ITER gyrotron was operated at a second frequency of 135 GHz for 0.1 s pulses and generated 0.8 MW power. This preliminary test has encouraged the IAP/GYCOM team to develop an optimized two frequency gyrotron employing a triode gun.

Operation of one of the 140 GHz, 1 MW gyrotrons of W7-X at IPP Greifswald (see Section 4.2.3) as a two-frequency gyrotron with a standard CVD-diamond window ($d = 1.799$ mm) delivered 0.41 MW in 10-s pulses at 103.8 GHz [34].

A MW-class two-frequency gyrotron (84 or 126 GHz, 2-s pulse duration, 1 MW power level) has been developed by the EU gyrotron team (see Section 4.3.3) [95]. Two tubes will be manufactured by THALES. The first gyrotron was already installed at the TCV site and successfully tested at short pulses (10 ms). It delivers 0.9 MW and 1.0 MW at the lower and higher frequencies, respectively, in a high-purity Gaussian wave beam [96].

5.3.2 Three- and Four-frequency gyrotrons in Japan

The QST gyrotron team found that the mode series of TE_{37,13} (203 GHz), TE_{31,11} (170 GHz), TE_{25,9} (137 GHz), TE_{19,7} (104 GHz) has very similar caustic radii as shown in table 6. In addition, these frequencies are located near the transparent frequencies of a single-disk diamond window with 1.853 mm thickness. In the mode converter design, conversion efficiencies of more than 97% were obtained from all the excited modes to a Gaussian output beam. The first gyrotron which employs this mode series was developed in 2009. Its outward appearance and dimensions are unchanged from the previous QST (JAEA) gyrotrons including the former TE_{31,8} mode ITER gyrotron. The corresponding design parameters are summarized in table 6. Basically, the beam radius in the cavity to excite the target mode is optimized using the gun field. The electron gun is a triode MIG type, which enables selection of the pitch factor of the electron beam for each operating frequency separately.

Table 6. Design parameters of QST multi-frequency gyrotron.

Frequency	203 GHz	170 GHz	137 GHz	104 GHz
Cavity Mode	TE _{37,13}	TE _{31,11}	TE _{25,9}	TE _{19,7}
Cavity Magnetic Field	7.98 T	.63 T	5.32 T	4.08 T
Gun Field	0.31 T	0.28 T	0.21 T	0.172 T
Beam Radius in Cavity	9.10 mm	9.13 mm	9.19 mm	9.25 mm
Beam Voltage	72 kV	72 kV	72 kV	72 kV
Anode Voltage	50 kV	42 kV	36 kV	28 kV
Beam Current	40 A	40 A	40 A	40 A
Pitch Factor	1.35	1.35	1.35	1.32
Oscillation Power	1.3 MW	1.3 MW	1.26 MW	1.12 MW

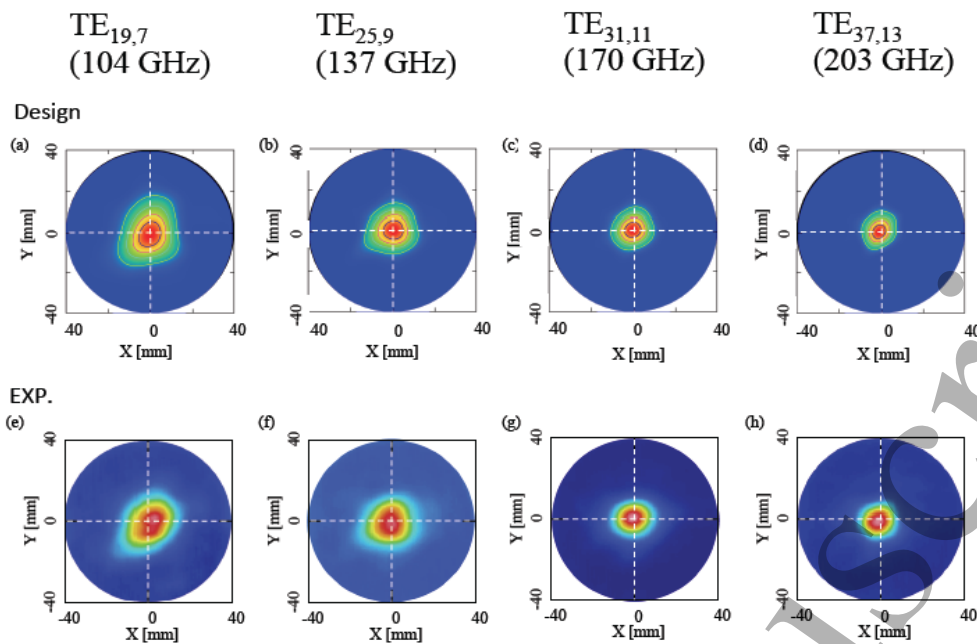


Figure 30. Designed and experimental RF intensity profiles at the output window of the QST multi-frequency gyrotron. The measured output powers and pulse durations are 1.0 MW (3 s) at 203 GHz, 1.2 MW (5 s)/1.0 MW (300 s) at 170 GHz, 1.0 MW (6 s) at 137 GHz and 1.0 MW (2 s) at 104 GHz.

Dual frequency operation was demonstrated as a first step [125]. Triple frequency operation (170 GHz, 137 GHz and 104 GHz) was obtained in 2012 [126]. After introducing an 8 T SCM, four-frequency operation was realized [108,127]. In figure 30, the RF intensity profiles at the window measured by an infrared camera are shown. 1 MW Gaussian mode output power was achieved for all four frequencies. Figure 31 shows the dependence of the 203 GHz output power and efficiency on the beam current. It should be noted that stable 50% high-efficiency operation in a very high order mode ($TE_{37,13}$) was achieved in a conventional hollow cylindrical cavity. The cavity magnetic field at 1 MW operation was approximately 7.9 T. Since the center of the Gaussian output beam is always at the center of the window, high efficiency coupling to the HE_{11} -mode waveguide was obtained for all four modes (frequencies) without control of the mirrors in the MOU [128]. If a 9.5 T magnet were available, 236 GHz ($TE_{43,15}$ mode) oscillation could be obtained.

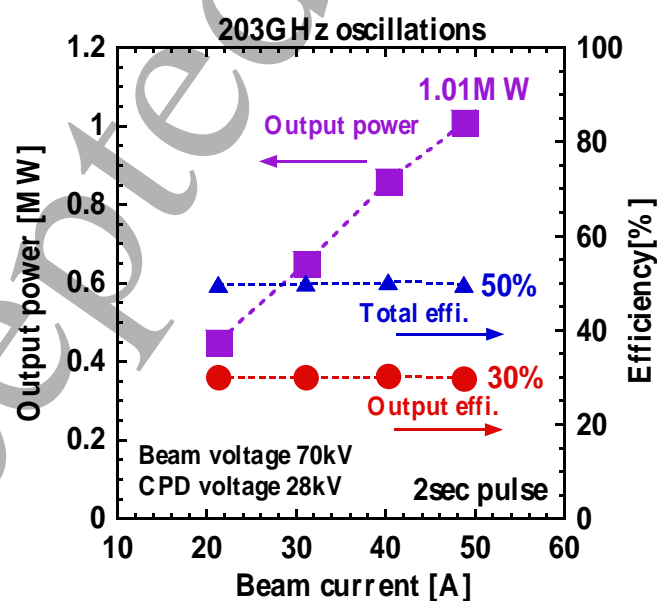


Figure 31. Measured output power and efficiency of 203 GHz operation of the QST gyrotron vs. beam current at a beam voltage of 70 kV with 28 kV collector depression voltage (2-s pulse length).

The 110 GHz QST gyrotron for JT-60SA obtained 1.9 MW for 1-s pulse operation utilizing the TE_{22,8}-cavity mode (see Section 4.2.1). In addition, oscillations of 1.3 MW for 1.3-s pulses at 138 GHz (TE_{27,10} mode) and 1 MW for 1-s pulses at 82 GHz (TE_{17,6} mode) have been demonstrated with this tube.

5.4 Stepwise frequency tunable gyrotrons

One of the major roles of local ECH&CD in ITER and other tokamaks is the suppression of Neoclassical Tearing Modes (NTMs) [5,104]. In order to compensate for the lack of current in the center (O-point) of a magnetic island, external current drive is required inside the island. The use of frequency step-tunable gyrotrons could greatly enhance the flexibility and performance of the ITER ECH&CD system. A system based on frequency step-tunable sources with frequency steps of 2-3 GHz could be used together with simple, fixed launcher structures without loss of performance. Because the magnetic field strength decreases toward the major radius direction in the case of tokamak, the power deposition point can be controlled by frequency control. As a reference, the power deposition point roughly moves ~10 cm with a frequency shift of 3 GHz in the plasma for ITER class tokamaks. Gyrotrons with broadband CVD-diamond windows and fast-tunable superconducting gyrotron magnets (sweeping speed 0.2 T/5 s corresponding to 1 GHz/s) would allow stepwise frequency tuning in a time scale of seconds over the full D-band (110-170 GHz).

One idea for a broadband high-power window is a double CVD-diamond disk window. By changing the width of the gap between the two diamond disks mechanically, the transmission efficiency can be optimized for each frequency. However, RF arcing due to standing waves between the two disks could be a problem. In addition, if used as a gyrotron output window, reflections could influence the search for optimum gyrotron operating parameters. A second idea is a Brewster window. When the RF beam, linearly polarized in the reflection plane, is injected with the Brewster angle defined by

$$\theta_B = \arctan \left(\sqrt{\frac{\varepsilon_1}{\varepsilon_2}} \right) = 67.2^\circ \text{ (for CVD diamond)}, \quad (11)$$

no reflection occurs over a wide range of frequencies. Here, ε_1 and ε_2 are the dielectric constant of the material and the atmosphere/vacuum, respectively. This type of window was first demonstrated on multi-frequency gyrotrons using an elongated silicon nitride disk [129,130]. A third possibility is a travelling wave window (see Section 5.4.2).

5.4.1 Fast frequency-tunable gyrotron in Japan

A cryogen-free SCM for fast frequency tuning has already been developed in Japan [59,131]. In this SCM, an additional superconducting sweeping coil is installed inside the main coil. The diameter of the room temperature bore is 240 mm, and the center magnetic field is 7 T. Using commercially available DC power supplies, cavity field sweeping is realized at 7 T over a range of 0.4 T, which corresponds to ~10 GHz shift, within 10 s. For example, around 0.125 T is required to switch between the modes TE_{31,8} (170 GHz) and TE_{30,8} (166.8 GHz) at optimum efficiency. In figure 32, the preliminary experimental results for the fast frequency control experiment are shown. Here, the beam voltage, V_b , is fixed at 71.0 kV, and the beam current is $I_b = 27.4$ A. The frequency shift between 170 GHz and 166.8 GHz was performed within 3.5 s. The oscillation modes are TE_{31,8} and TE_{30,8}, respectively. Power and efficiency without a depressed collector are 615 kW (32 %) and 538 kW (27 %), respectively. This could be beneficial to plasma stabilization experiments [126]. In addition, by adding electron beam voltage control, fast frequency change can be realized.

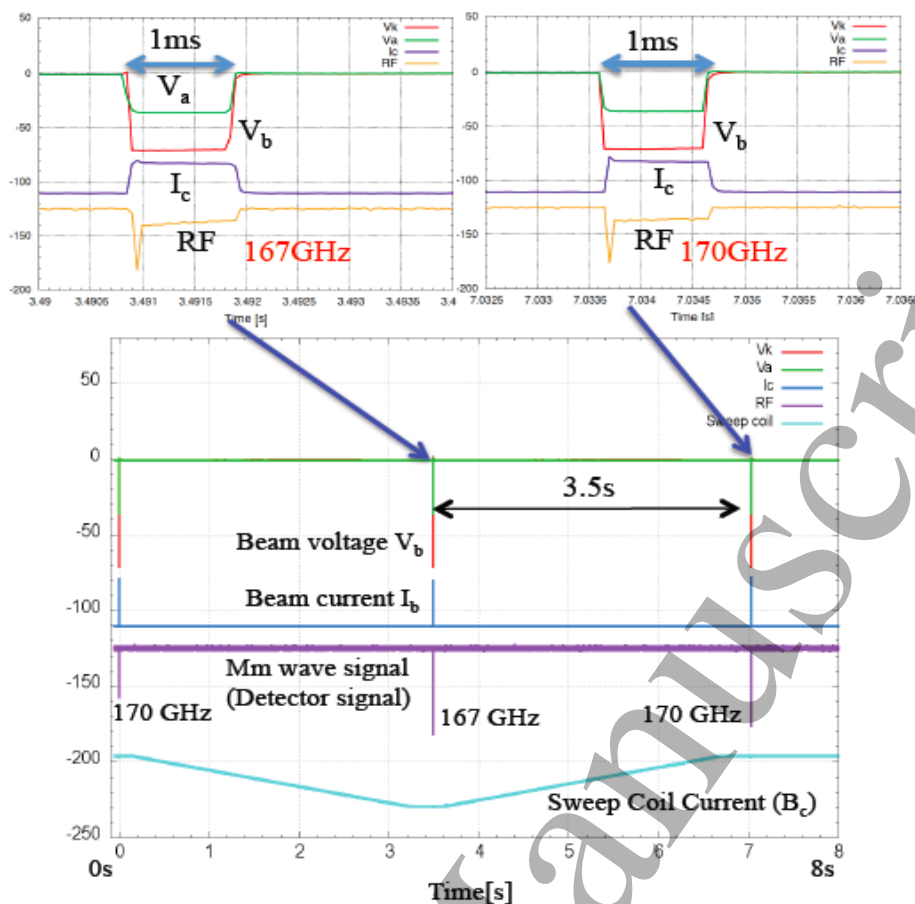


Figure 32. Time traces of beam voltage V_b , beam current I_c , mm-wave diode signal and sweeping coil current (which corresponds to a change in the cavity magnetic field) of the $TE_{31,8}$ -mode QST gyrotron. At the bottom of the sweeping current, the $TE_{30,8}$ mode (166.8 GHz) is excited. The duration of the pulses is 1 ms as indicated in the upper figures.

5.4.2 Frequency-tunable gyrotrons in Russia

A GYCOM 140 GHz $TE_{22,10}$ -mode gyrotron was operated at 0.8 MW in 50-150 ms pulses utilizing a BN Brewster window at 11 frequencies (modes) between 104 and 143 GHz [107].

At present, GYCOM/IAP is developing in collaboration with IPP Garching and KIT, an industrial, frequency-tunable 1 MW gyrotron with almost 50% efficiency (SDC) for the new ASDEX Upgrade ECH system [94]. A four-frequency tube (105, 117, 127 and 140 GHz) with the $TE_{22,8}$ cavity mode at 140 GHz, delivered 0.8 MW at 105 GHz and 0.9 MW at 140 GHz in 10-s pulses (two-frequency gyrotron) (see 5.3.1). The single-disk CVD-diamond window has maximum transmission for these two frequencies. After the installation of a circularly-brazed CVD-diamond Brewster window with specific internal and external mirrors mounted close to the window disk, the GYCOM/IAP group operated this gyrotron also at the two intermediate frequencies. However, the CVD-diamond disk broke due to successive RF arcing in front of the disk. Therefore, GYCOM is now developing a tunable travelling-wave window consisting of two CVD-diamond disks and two mirrors (see figure 33) [132]. The principle of the travelling wave window can be explained by figure 33. The two windows (shown by green cuffs) and two adjustable mirrors form a ring resonator with a travelling wave. The system has zero reflections at the resonant frequency. At non-resonant frequencies some reflection from the resonator occurs, but the reflected wave does not propagate back into the cavity and does not disturb the gyrotron operation. It is directed via a relief window into a relief load. In addition, this window unit is transparent for the frequencies where the disks are transparent. This ring resonator mock-up with typical gyrotron-wave-beam window sizes was tested at low power and found to be an appropriate solution [132].

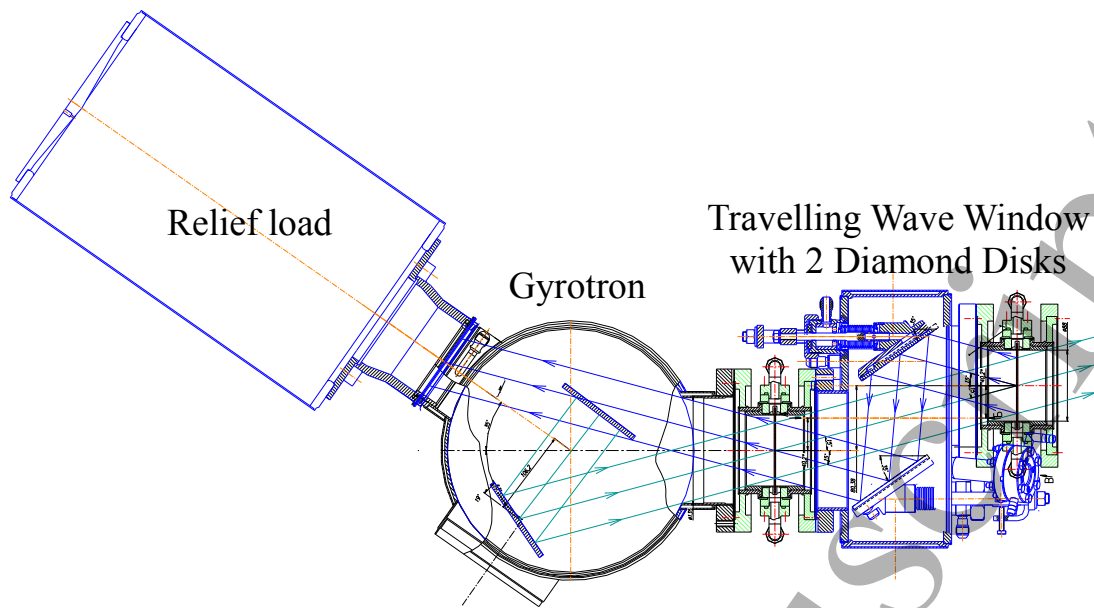


Figure 33. GYCOM tunable travelling-wave window employing two standard 106-mm-diameter CVD-diamond disks, two tunable mirrors and a calorimetric load at the relief window.

5.4.3 Frequency-tunable gyrotrons in EU

Already in the 1990's, D-band short-pulse (1 ms) frequency tunable megawatt-class gyrotrons with broadband SiN Brewster-angle windows were tested at KIT (FZK) [129,130]. In the conventional cylindrical -cavity tube (114 – 166 GHz, $TE_{22,6}$ cavity mode at 140 GHz), in which such frequency tuning was realized, the frequency spacing was 3.7 GHz [41], whereas the different modes of the coaxial-cavity tube (133 – 148 GHz, $TE_{28,16}$ cavity mode at 140 GHz) had a frequency separation of 2.2 GHz [105]. In addition, the 1 MW $TE_{22,6}$ -mode gyrotron was investigated with respect to fast-frequency tunability between 5 modes in the 15 GHz-bandwidth range from 132.6 to 147.4 GHz [133]. For that purpose, the gyrotron was equipped with a special hybrid-magnet system consisting of the SCM in the cryostat and additional normal-conducting (NC) copper magnets with a fast time constant at the cavity and cathode locations. Special problems due to the magnetic coupling between the different magnets were investigated by calculation and experiment. Making use of these investigations different current regulation schemes for the NC magnets were implemented and tested experimentally. Finally, megawatt-level step-tuning operation between the modes from $TE_{20,6}$ to $TE_{24,6}$, in time steps of 1 s, was achieved.

Currently, KIT is developing a step-frequency tunable D-band MW gyrotron using an elliptically brazed CVD-diamond window. As in the Russian tube, the cavity mode at 140 GHz is the $TE_{22,8}$ mode. The dimensions of the diamond disk are 139 x 95 x 1.7 mm (figure 34) [134]. The elliptically shaped disk was brazed at the Brewster angle (67.2°) together with two OFHC copper cuffs with 49-mm inner diameter and 0.5-mm wall thickness. The total length of the window system is 206 mm. A proper braze design is the key to success. It must withstand the significantly different thermal expansion coefficients for diamond and copper (1:17). The diamond disk and the copper cuffs were brazed at a temperature of about 800°C , while the system is used at room temperature. Extensive 3D-FEM thermo-mechanical calculations (ANSYS) indicated that the stress in the disk and the copper cuffs did not exceed critical values. The distribution of the stress on the top side of the disk showed a maximum value of less than 150 MPa, which is considered as a conservative permissible stress (ultimate strength of diamond is 450-500 MPa). This value is higher by a factor of 1.4 compared to a circular disk. The equivalent von Mises stress on the copper cuffs at 20°C is 45 MPa, whereas the ultimate strength is 250 MPa. Low-power measurements confirm a transmission efficiency of more than 99%.



Figure 34. CVD-diamond disk and elliptically brazed Brewster window at KIT [132] (© 2014 IEEE. Reprinted, with permission from [134] Gantenbein G et al 2014, IEEE Trans. on Electron Devices 61, 6, 1806).

Table 7. Cavity modes, electron beam energy, beam current, output power and efficiency of KIT step-tunable megawatt-class D-band gyrotron with CVD-diamond Brewster window (pulse length = 3 ms).

Mode	Frequency [GHz]	E_{beam} [keV]	I_{beam} [A]	Power [kW]	Efficiency [%] (without SDC)
TE _{19,6}	111.6	84.1, short cavity	41	830	24.1
TE _{20,7}	124.2	71.6	42.5	1004	33.0
TE _{21,7}	127.5	68.8	43	1035	35.0
TE _{22,8}	140.1	69.1	45	1150	37.0
TE _{23,8}	143.4	67.6	44	1210	40.5
TE _{24,8}	146.7	68.2	42.5	1200	41.4
TE _{24,9}	155.9	85.2, short cavity	43	1000	27.3
TE _{25,9}	159.2	75.5	44	1093	32.9
TE _{26,9}	162.6	77.4	42	1200	36.9
TE _{27,9}	165.9	78.3	44	1100	31.9
TE _{28,9}	169.2	74.9	43	1150	35.7

The step-frequency tunable KIT gyrotron has been operated in 3-ms-pulses with 11 modes in the frequency range starting from 111.6 to 169.2 GHz. The corresponding cavity modes, electron beam parameters, output powers and efficiencies (without depressed collector) are summarized in table 7 [135]. The results at 111.6 and 155.9 GHz were obtained using a shorter cavity with lower diffractive Q (850 compared to 1200).

5.5 Coaxial-cavity gyrotrons

To keep the number of required gyrotrons and magnets as low as possible, to reduce the costs of future fusion reactor ECH&CD systems and to allow compact poloidal launchers for plasma stabilization, 2 MW power per tube is desirable. Conventional, cylindrical gyrotron cavities are not suitable for very high-frequency (e.g. 204 GHz for DEMO), high-power applications because of high Ohmic wall losses

1
2
3 and/or mode competition problems. However, in coaxial cavities the existence of the longitudinally-
4 corrugated inner conductor reduces the problems of mode competition and limiting current, thus
5 allowing one to use even higher order modes with lower Ohmic attenuation than in cylindrical cavities
6 [136]. In addition, the inner rod enables a specific voltage depression scheme for energy recovery and
7 ultra-fast frequency step tuning just by applying an appropriate voltage to this coaxial insert. CVD-
8 diamond windows with a transmission capability of 2 MW, CW are feasible (see Section 3.4).
9

10 Successful activities on the development of 1.5 – 2 MW short-pulse gyrotrons with coaxial cavities were
11 conducted at IAP Nizhny Novgorod ($TE_{28,16}$ at 140 GHz [137]) and KIT (FZK) Karlsruhe ($TE_{28,16}$ at
12 140 GHz and $TE_{31,17}$ at 165 GHz) [136,138]. In single-pulse operation of the 165 GHz tube, the pulse
13 length was extended up to 17 ms. At $V_b = 93$ kV and $I_b = 84$ A a maximum RF output power as high as
14 2.2 MW was achieved with an efficiency of 28 %. Operation with a single-stage depressed collector was
15 performed at an efficiency of 49 % and an output power of 1.5 MW.

16 A 2 MW, CW, 170 GHz coaxial-cavity gyrotron operating in the $TE_{34,19}$ mode for ECH&CD in ITER
17 was under development in the EU by EGYC [72]. The design of critical components like the electron
18 gun, beam tunnel, cavity and quasi-optical mm-wave output system was studied in a short-pulse coaxial
19 gyrotron (pre-prototype) at KIT. At a magnetic field of $B = 6.87$ T a maximum mm-wave output power
20 $P_{out} = 2.2$ MW was obtained at $V_b = 93$ kV and $I_b = 80$ A with an efficiency of around 30% at 1 ms pulse
21 duration in non-depressed collector operation [139]. If a CVD-diamond window had been installed
22 instead of the fused silica window, the output power would have been 2.3 MW with an efficiency of
23 31 %, due to lower mm-wave absorption in diamond. The Gaussian output mode purity was almost 96%.

24 RF tests with an industrial prototype gyrotron (THALES) were done at the EU test facility at SPC
25 (CRPP) Lausanne in December 2011 [72]. This tube did show excellent voltage stand-off. It was
26 possible to excite the nominal operating $TE_{34,19}$ mode. The output RF beam profile was in good
27 agreement with the expected profile. The output power reached a level of almost 2.1 MW in short-pulse
28 (1 ms) operation with SDC operation corresponding to 46 % efficiency. The results were achieved after
29 only 4 days of operation without any further optimization. However, the next day when an internal
30 water-cooled, alumina-pipe-stray-radiation load broke, the tube was lost and the EU ITER gyrotron
31 development strategy changed to the back-up solution of a 1 MW conventional cylindrical cavity
32 gyrotron operating in the $TE_{32,9}$ mode.
33

34 Nevertheless, the development of multi-megawatt coaxial-cavity gyrotrons will continue in the EU,
35 because very-high frequency gyrotrons (e.g. 204 or 238 GHz) for ECH and efficient non-inductive
36 ECCD in future nuclear fusion reactors like DEMO will likely require coaxial cavities to generate unit
37 powers of more than 1.5 MW. Currently, a longer-pulse (100 ms) version of this 170 GHz, 2 MW
38 coaxial-cavity gyrotron is under test at KIT (see figure 35) [140,141]. The measured mm-wave output
39 power (ms pulses) versus the cathode voltage at $I_b = 81$ A is shown in figure 36 [141]. The figure also
40 contains the results of numerical simulations performed with the KIT self-consistent multi-mode code
41 including 6 % rms transverse electron velocity spread. The agreement between experiment and
42 simulations is very good if approximately 5 % of the generated output power in the nominal mode is
43 assumed to be lost inside the tube due to stray radiation, Ohmic losses and absorption in the output
44 window. After further parameter optimization, the RF power was increased to 2.2 MW at an efficiency
45 of approximately 33 % (without SDC).
46
47
48

49 In order to extend the range of stable single-mode operation at very high frequencies and multi-megawatt
50 power level, the outer cavity wall could be equipped with mode-converting corrugations, which
51 transform the azimuthal satellites of the operating cavity mode to low-Q modes, that are strongly
52 disturbed by the inner conductor. Such an experiment was conducted at IAP in 2002 [142], employing
53 the co-rotating $TE_{+28,16}$ -cavity mode at 140 GHz in a 1 MW short-pulse gyrotron. In this case, 44
54 longitudinal, rounded vanes (0.2 mm deep) in the outer cavity wall converted the co-rotating $TE_{+29,16}$
55 and $TE_{+27,16}$ satellite modes to the degenerate counter-rotating modes $TE_{-15,20}$ and $TE_{-17,19}$, respectively.
56 Conversion to counter-rotating modes is utilized to guarantee only negligible unwanted conversion of
57 the operating mode. In [143], a numerical code based on the spatial harmonics method is used to study
58 this method in detail. However, if step-wise frequency tuning is required, such cavities would provide a
59 mode spectrum with two times larger frequency separation compared to cavities with smooth outer wall.
60

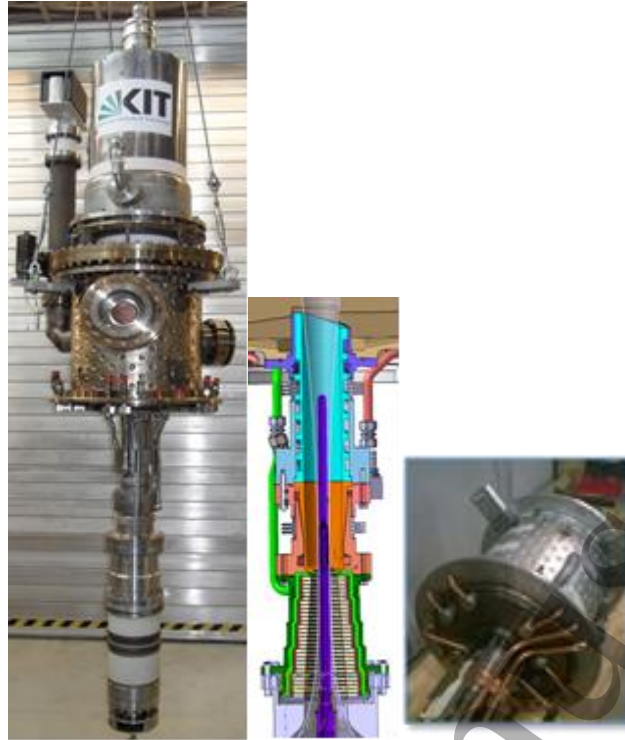


Figure 35. Photo of the upgraded KIT 170 GHz, 2 MW coaxial-cavity pre-prototype to operate at pulse lengths up to 100 ms (left). Sketch of the key components which have been upgraded with advanced cooling systems (middle). Upgrade of the mirror box showing the cooling system (right).

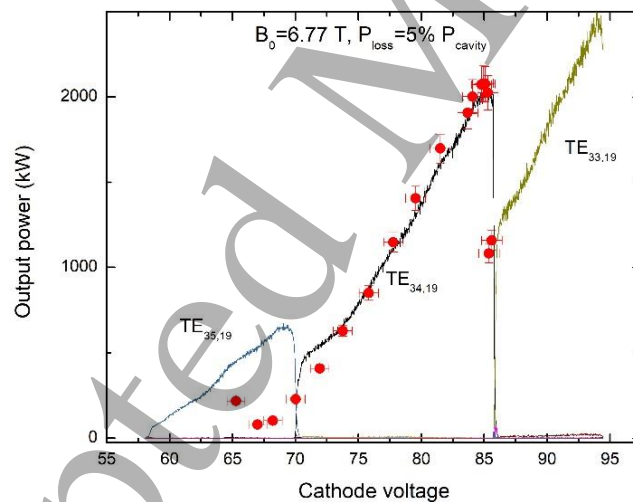


Figure 36. Measured (points) and calculated (solid lines) output power of the KIT coaxial-cavity prototype short-pulse gyrotron vs. beam voltage at $I_b = 75 \text{ A}$ and cavity magnetic field of 6.77 T.

To support at KIT the future development of CW gyrotrons with an output power of up to 4 MW at frequencies up to 240 GHz, the new gyrotron test facility Fusion Long Pulse Gyrotron Laboratory (FULGOR) was installed, which is capable of up to 10 MW CW operation [119]. The main HV DC power supply, delivered in late 2017 by Ampegon AG (Turgi, Switzerland) and accepted in 2018, provides voltages and currents up to 90 kV/120 A for 3600 s at 50 % duty cycle and 130 kV/120 A in short pulses (5 ms/25 % duty cycle). There is the possibility for up to 10 intermediate voltage taps for multi-stage depressed collector operation, freely selectable in 1.2 kV steps. A 10.5 T cryogen-free gyrotron SCM with 261 mm warm bore and dipole coils for transverse electron beam alignment was ordered from Tesla Engineering Ltd., Storrington, UK.

5.6 Injection locking of gyrotrons

At IAP Nizhny Novgorod there are new developments in phase locking megawatt-class gyro-oscillators [144-146]. Starting from a 1.5 MW, 170 GHz, $TE_{28,12}$ -mode tube with 2.5 s pulse length, 49 % efficiency (with SDC) and 97 % Gaussian-beam output, a gyrotron operating efficiently in modes of both rotations was developed and tested in proof-of-principle experiments. The gyrotron operation can be switched between two modes: co- and counter-rotating $TE_{\pm 28,12}$ at 170 GHz, by adjusting a cathode coil to select the mode rotation. A new synthesized quasi-optical mode converter composed of 3D metal reflectors provides output coupling for the generated waves in the form of two paraxial Gaussian wave beams, each of them corresponding to a specific direction of mode rotation (see figures 37 and 38). The measured gyrotron output power (up to 2 MW in short-pulse operation), interaction efficiency (34 %, without SDC) and diffraction losses in the mode converter ($< 2\%$) agree well with the design values (see figure 39). The new gyrotron scheme allows a basic enhancement of the device parameters, the possibility of electronic switching of the output wave beam direction, frequency stabilization by reflection, and the possibility of providing an effective approach to enable frequency and phase locking of a gyrotron-oscillator (injection locking). The latter advance could lead to very efficient single-mode operation in very high order modes (high-frequency 1.5 MW-class gyrotrons with conventional hollow cavity), stabilized by an external signal while the electron beam parameters are not so stable, and the possibility of making several individual gyrotrons coherent. In addition, the possibility of very precise stabilization of a gyrotron-driver was demonstrated [124].

To accomplish phase or frequency locking, the counter-rotating input beam (see figure 37 (b)) is converted to the counter-rotating $TE_{-28,12}$ mode, which by reflection at the cutoff section of the gyrotron cavity is converted to the operating co-rotating $TE_{+28,12}$ cavity mode. The input and output wave beams pass through the gyrotron output window at an angle of ± 10 deg. with respect to the window normal.

The first experiments on gyrotron frequency stabilization by optimum reflection were very encouraging. For a rather high voltage variation of 95-100 kV the frequency was stable to within 2 MHz.

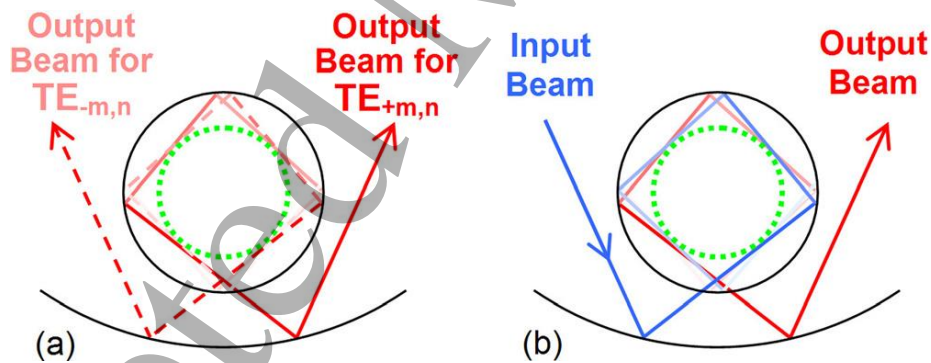


Figure 37. Two operation regimes of mode converter: (a) conversion of both the co- and counter rotating modes and (b) frequency/phase locking regime (Reproduced from [144] Chirkov AV et al 2015, Applied Physics Letters 106, 263501, with permission of AIP Publishing).

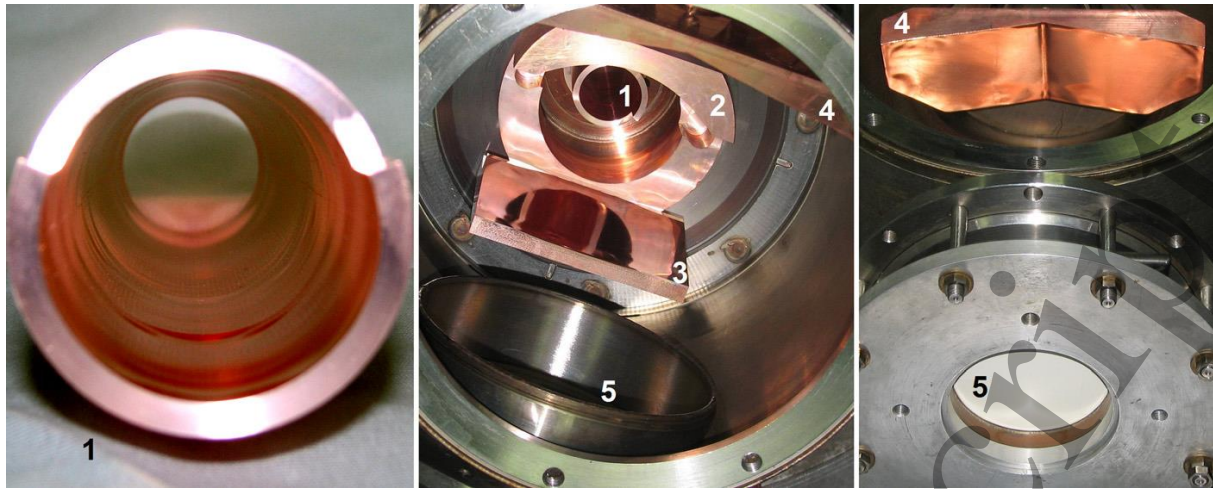


Figure 38. Mode converter for co- and counter-rotating cavity modes: (1) waveguide launcher, that has a vertical plane of symmetry, (2) parabolic mirror, (3) and (4) matching mirrors with non-quadratic surface contour functions, and (5) BN vacuum window (Reproduced from [144] Chirkov AV et al 2015, Applied Physics Letters 106, 263501, with permission of AIP Publishing).

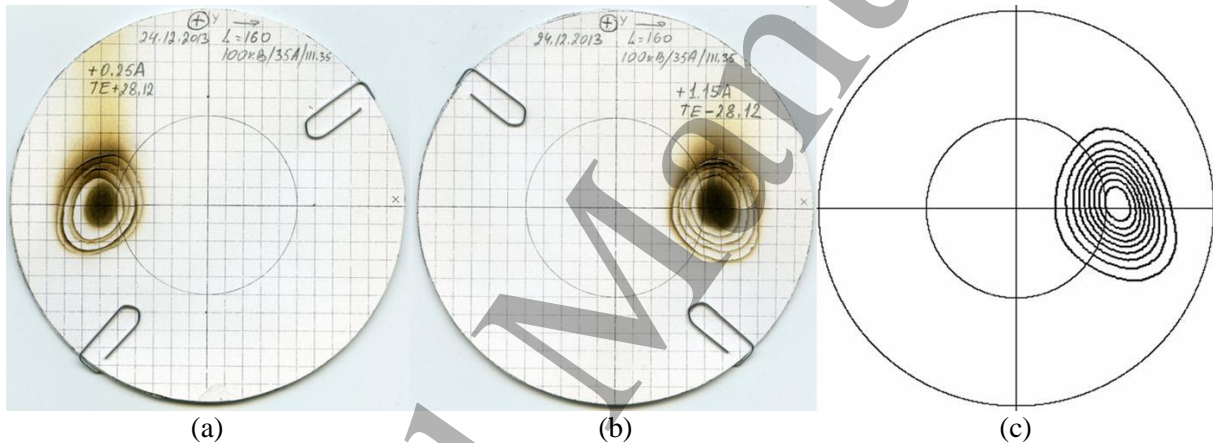


Figure 39. (a) and (b) Stacks of five burn patterns (with different exposition times) of the gyrotron output beam for co- and counter-rotating cavity modes at the distance of 160 mm from the gyrotron window, and (c) simulated beam intensity pattern in the same scale (Reproduced from [144] Chirkov AV et al 2015, Applied Physics Letters 106, 263501, with permission of AIP Publishing).

5.7 Efficiency and RAMI

Efficiency enhancement via multi-stage depressed collectors, fast oscillation recovery methods and RAMI will be discussed in this section.

5.7.1 Multi-stage depressed collector

One promising approach for increasing the total efficiency of fusion gyrotrons above 60 % is to use a multi-stage depressed collector (MDC). That technology is well known from highly efficient traveling wave tubes (TWT) for space applications [147]. Those collectors use electrostatic or magnetic focusing to separate electrons with different energies within the spent electron beam in several intermediate steps of depression voltage along the electron beam axis. For gyrotrons there are also two known theoretical MDC concepts: one is to make use of the non-adiabatic electron trajectories in a strong magnetic field [148]; the other is to utilize the $E \times B$ drift of the electrons in crossed electric and magnetic fields [149]. Even though several considerations for gyrotron MDC designs exist in the literature, there has been no implementation of that technology in an experimental gyrotron. In the frame of EUROfusion, at KIT the

MSDC technology shall be pushed significantly forward. Initial steps towards new, experimentally feasible $E_{\phi} \times B_z$ drift MDC design concepts have already been undertaken [150].

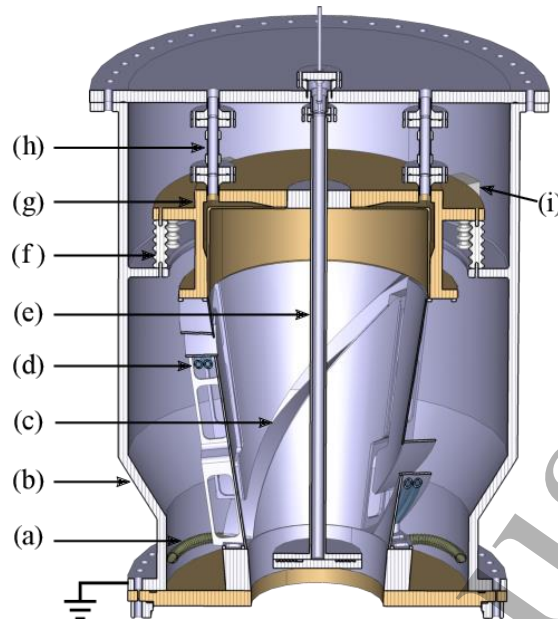


Figure 40. Cross section of the mechanical design of the advanced $E_{\phi} \times B_z$ drift MDC. (a) Water cooling feed through pipes. (b) Grounded vacuum vessel. (c) Helical electrode insulation gap. (d) Water cooling pipes. (e) Grounded coaxial insert. (f) Insulators. (g) Water cooled cap of the second stage. (h) Isolated water feed through. (i) Ceramic stabilization blocks (Reproduced from [151] Wu C et al 2019, *Phys. Plasmas* **26**, 013108, with permission of AIP Publishing).

A realistic and feasible mechanical design is shown in figure 40 [151]. It is based on the typical isolation scheme of fusion gyrotrons, where the cavity is at positive body potential while the mirror-box and the collector outer case (here, the vacuum vessel (b)) are grounded to create a depression voltage for the first stage. Water cooling is considered even in this short-pulse design, in order to increase the duty cycle. The surfaces of the first stage are thin metal plates supported by a metal frame. Beneath the helical electrode insulation gap (c) where slow electrons impact, are the cooling pipes (d) for the first stage. The cooling water is fed through the pipes (a). (e) is the coaxial insert, which is also grounded and hung from the top of the vacuum envelope.

The second stage has a potential of approximately -12 kV. It is supported by several insulators (f). (g) is the “cap” of the second stage, which is also water cooled. The water is fed via the ceramic pipe (h), which also isolates the ground potential from the potential of the second stage. To protect the second stage from harmful transverse motions, which could break the insulators, a few ceramic blocks (i) are installed to fix the transverse position of the second stage.

5.7.2 Fast oscillation recovery methods (re-start during the shot)

Maximum possible ECH&CD system power and operational stability are very important performance parameters. However, approaching the maximum gyrotron output power, undesired satellite modes are excited simultaneously with the operating main cavity mode [51]. This increases the stray radiation inside the tube and loss of the oscillating mode due to mode switching becomes more likely. The usual solution is a trade-off between output power and reliability by operating the gyrotrons below their maximum output power to guarantee a safety margin. An innovative solution has been introduced in the ECH system of W7-X [152,153]. It consists of a fast gyrotron controller (MORE) with a mode-loss precursor feedback and in case this stabilization fails, a fast, automated mode recovery within less than 1 ms is obtained by reducing the body voltage by approximately 9 kV. Then the body voltage is increased

again, to return to the maximum output power. Figure 41 shows a 20-s pulse with 820 kW RF power (lower trace). Using the MORE controller, the average output power could be increased to 875 kW (upper trace).

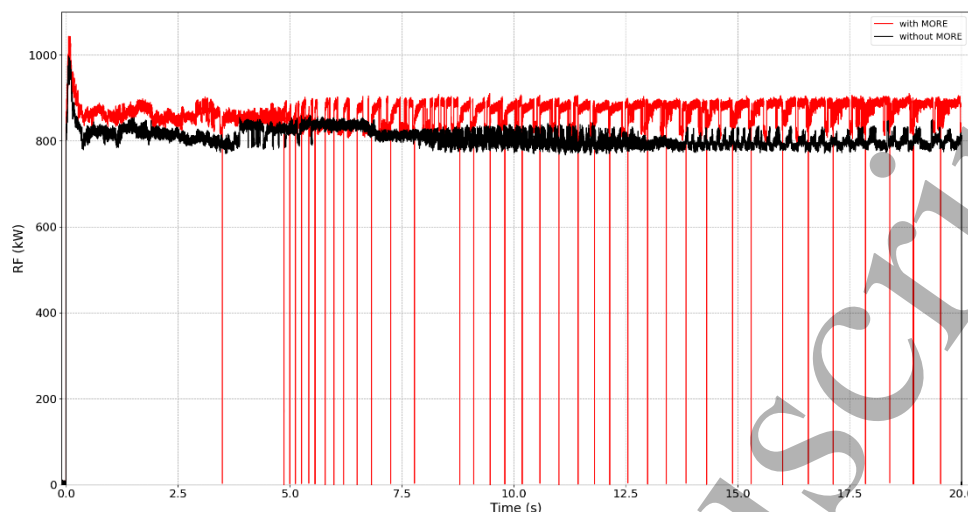


Figure 41. Fast gyrotron oscillation recovery of 140 GHz W7-X gyrotron [153]. Red pulse trace with MORE and black pulse trace without MORE.

5.7.3 Reliability, Availability, Maintainability and Inspectability (RAMI)

In a fusion power plant, where all heating and current drive equipment must meet prescribed functions, the issues of RAMI become an integral part of the functional requirement. In present laboratory fusion plasma devices one is usually just performing experiments with whatever power is available on the allocated days: the power requirement is often adapted to the individual gyrotrons of the ECH&CD system. Of course, fast gyrotron oscillation recovery improves the situation (see 5.7.2). In a fusion power plant, an insufficient H&CD power level may jeopardize the pulse, leading to the premature termination of the plasma discharge (assuming a soft landing is possible) and consequently to the disruption of the electricity supply to the grid.

True RAMI studies on heating systems are scarce due to the non-availability of data on large systems in reactor like environment or even with large systems (many tens of MW of installed power). Experience with the 24 MW ITER ECH&CD system will be of great importance to realistic RAMI studies.

The present available data on megawatt-class gyrotrons often reports the number of successful shots at prescribed power level and pulse length. For example, the reliability requirement for the ITER tubes is $\geq 95\%$, defined on 20 pulses of full power and 500 s pulse length. In case of a mode loss occurring during the pulse, this pulse would still be considered successful if full power generation could restart quickly enough to have the nominal output power during a minimum of 95% of the 500-s pulse.

For simulation of ITER operation with the Japanese 170 GHz gyrotron, 0.8 MW pulses at 600 s pulse length were repeated with an interval of 20 ~ 30 min. 72 shots of 88 trials were very stable over the full pulse duration. The other pulses were interrupted by internal arcing, etc. (see 4.1.2). Tests at 1 MW output power with the Russian ITER gyrotron at pulse durations of 500 s and 1000 s showed a reliability of gyrotron operation $\geq 95\%$ (see 4.1.3). The 140 GHz THALES gyrotron for W7-X delivered 0.7 MW pulses with 180 s pulse duration at 98 % reliability [90].

The very high RAMI level required for future fusion power plant gyrotrons, e.g. for DEMO, suggests the need for further optimization of all the critical tube components. In addition, advances with respect to robustness against manufacturing tolerances and maintainability are necessary.

6. Conclusions

The state-of-the-art and recent outstanding activities in the field of high-power gyrotron development for magnetic confinement fusion applications have been summarized. Since the early 1990's, gyrotron research and development advanced significantly, and progress is still underway. This is the reason why ECH&CD mutated from being a stepchild in the family of plasma heating methods to being a major player in the field. Rapid progress in 1 MW-class long-pulse operation at 140 and 170 GHz resulted in the facts that ECH is the only 10 MW long-pulse heating system of W7-X, will be the first auxiliary heating method used at ITER (24 MW), is utilized in all major plasma confinement devices, with the exception of JET, and that ECH&CD is foreseen in all the different design proposals for a future DEMO reactor. Table 8 summarizes the parameters of running, prepared and foreseen multi-megawatt ECH&CD systems with frequencies higher than 77 GHz. Sub-THz gyrotrons are being used for collective Thomson scattering (CTS) diagnostics. The next targets are tubes with higher frequencies for DEMO, multi-frequency (multi-purpose) gyrotrons, and stepwise frequency tunable tubes for plasma stabilization with

Table 8. Features and parameters of running and foreseen (*italic letters*) multi-megawatt ECH&CD systems with frequencies higher than 77 GHz.

Plasma Device Type	Institution (Site)	ECH Power [MW]	Frequency [GHz]	Pulse Duration [s]	Energy at Plasma [MW x s]	Company/ Institution
ASDEX-U Tokamak [154]	IPP Garching	8.0 (8x1.0)	140+105	10.0	4.5 x 10.0 <i>6.4 x 10.0</i>	GYCOM/IAP
DIII-D Tokamak [155]	GA San Diego	3.0 (3x1.0) 1.5 (1x1.5) <i>4.0 (4x1.0)</i>	110 117.5 <i>110</i>	5.0 5.0 <i>5.0</i>	2.35 x 5.0 1.0 x 2.0 <i>3.2 x 5.0</i>	CPI CPI <i>CPI</i>
EAST Tokamak [156]	IPP Hefei	4.0 (4x1.0)	140	1000	1.4 x 100 <i>3.6 x 1000</i>	GYCOM/IAP (2 Tubes) CPI (2 Tubes)
<i>ITER Tokamak</i>	<i>Cadarache</i>	<i>24.0 (24x1.0)</i>	<i>170</i>	<i>1000</i>	<i>20.0 x 1000</i>	<i>GYCOM/IAP, CETD/QST, EU, INDIA,</i>
<i>JT 60SA Tokamak</i>	<i>QST Naka</i>	<i>4.0 (4x1.0) later</i> <i>9.0 (9x1.0)</i>	<i>138+110+82 multi-freq. gyrotron</i>	<i>5.0, 100 later</i> <i>100</i>	<i>1.5 x 5.0 + 1.5 x 100 later</i> <i>7.0 x 100</i>	<i>CETD/QST</i>
KSTAR Tokamak [157]	NFRI Daejeon	0.5 (1x0.5) 1.0 (1x1.0) 2.0 (2x1.0)	84 110 140+105	2.0 5.0 300.0	0.3 x 2.0 0.5 x 2.0 0.7 x 70.0	CPI GYCOM/IAP GYCOM/IAP
TCV Tokamak [158]	SPC Lausanne	1.5 (2x0.75) 1.5 (3x0.5) <i>2.0 (2x1.0)</i>	82.7 118 <i>126+84</i>	2.0 2.0 2.0	1.3 x 2.0 1.3 x 2.0 <i>1.8 x 2.0</i>	GYCOM/IAP THALES/EGYC <i>THALES/EGYC</i>
T-10 Tokamak [159]	NRC KI Moscow	1.0 (2x0.5) 1.7 (2x0.85) <i>1.2 (1.2x1.0)</i>	129 140 <i>140</i>	0.5 0.5 <i>10.0</i>	0.8 x 0.4 1.6 x 0.4 <i>1.1 x 1.0</i>	GYCOM/IAP
<i>T-15MD Tokamak</i>	<i>NRC KI Moscow</i>	<i>1.0 (1x1.0)</i>	82.9	<i>20.0</i>	<i>0.95 x 20.0</i>	<i>GYCOM/IAP</i>
LHD Stellarator [160]	NIFS Toki	3.9 (3x1.3) 2.2 (2x1.1)	77 156	5.0 5.0	3.5 x 2.0 1.9 x 2.0	CETD/UNIV. TSUKUBA
W7-X Stellarator [7]	IPP Greifswald	10.0 (10x1.0)	140	5.0 <i>1800</i>	8.0(5.0)x5.0(31) <i>8.0 x 1800</i>	THALES/KIT (9 Tubes) CPI (1 Tube)

fixed launching antennas. Injection-locked and coaxial-cavity gyrotrons are candidates for 1.5 - 2 MW output power per tube. Development challenge continue since efficiency enhancement via multi-stage depressed collectors, fast oscillation recovery methods and RAMI are absolutely necessary requirements for future thermonuclear fusion power plants.

Acknowledgments

The authors would like to thank the members of their related fusion gyrotron research and development teams and companies, EGYC with F4E and THALES in Europe, at IAP with GYCOM in Russia and at QST and University of Tsukuba with CTED in Japan for their continuous excellent R&D works. We would also like to thank John Lohr from GA for giving us an update of the status of the CPI development of 110 GHz and 117.5 GHz gyrotrons for the ECH&CD system at DIII-D.

The author's have confirmed that any identifiable participants in this study have given their consent for publication.

References

- [1] Freiberg J 2007, *Plasma Physics and Fusion Energy* (Cambridge University Press), pages 537-540
- [2] Wagner F et al 2010, *Plasma Physics and Controlled Fusion* **52**, 124044
- [3] ITER Physics Basis 1999, *Nucl. Fusion* **39**, 2496
- [4] ITER Physics Basis 2007, *Nucl. Fusion* **47**, 385
- [5] Kikuchi M , Lackner K and Tran MQ, eds, 2012, <http://www-pub.iaea.org/books/IAEABooks/8879/Fusion-Physics>, Chapter 6
- [6] Poli E et al 2013, *Nucl. Fusion* **53**, 013011
- [7] Wolf RC, 2019, *Plasma Physics and Controlled Fusion* **61**, 014037
- [8] Omori T et al 2015, *Fusion Eng. and Design* **96-97**, 547
- [9] Martin YR et al 2008, *J. Phys. Conf. Ser.* **123.1**, 012033
- [10] Vincenzi P et al 2017, *Fusion Eng. and Design* **123**, 473
- [11] Goodman TP et al 2011, *Phys. Rev. Lett.* **106**, 245002
- [12] Henderson MA et al 2008, *Nucl. Fusion* **48**, 054013
- [13] Granucci G et al 2017, *Nucl. Fusion* **57**, 116009
- [14] Alberti S et al 2017, *EPJ Web of Conferences* **157**, 03001
- [15] Edgcombe CJ, ed. 1993, *Gyrotron oscillators – their principles and practice*, Taylor & Francis, London
- [16] Kartikeyan MV, Borie E and Thumm MKA 2004, *Gyrotrons – High power microwave and millimeter wave technology*, Springer, Berlin
- [17] Nusinovich G 2004, *Introduction to the physics of gyrotrons*, The Johns Hopkins University Press, Baltimore and London
- [18] Benford J, Swegle J and Schamiloglu E 2007, *High-power microwave sources*, 2nd Ed., Taylor & Francis, New York, London
- [19] Litvak A, Sakamoto K and Thumm M 2011, *Plasma Physics and Controlled Fusion* **53**, 124002
- [20] Nusinovich GS, Thumm MKA and Petelin, MI 2014, *J. Infrared, Millimeter, and Terahertz Waves*, **35**, 4, 325
- [21] Thumm M 2014, *IEEE Trans. on Plasma Science* **42**, 3, 590
- [22] Thumm M 2014, *J. Infrared, Millimeter, and Terahertz Waves*, **35**, 12, 1011
- [23] Tsimring SE 2007, *Electron beams and microwave vacuum electronics*, John Wiley & Sons, Hoboken, NJ, USA
- [24] Kuftin AN et al 1999, *Int. J Infrared and Millimeter Waves* **20**, 381
- [25] Tsimring SE 2001, *Int. J Infrared and Millimeter Waves* **22**, 1433
- [26] Pagonakis IGr, Illy S and Thumm M 2016 *Physics of Plasmas* **23**, 083103
- [27] Gantenbein G et al. 2010, *IEEE Trans. on Plasma Science* **38**, 1168
- [28] Yu J, Antonsen TM and Nusinovich GS 2010 *IEEE Trans. on Plasma Science* **38**, 1193
- [29] Sakamoto K et al 2003, *Nucl. Fusion* **43**, 729
- [30] Vlasov SN, Zagryadskaya LI and Petelin MI 1975 *Radio Eng. Electron. Physics* **20**, 14
- [31] Thumm MK and Kasperek W 2002, *IEEE Trans. on Plasma Science* **30**, 755

- [32] Denisov GG et al 1992, *Int. J. Electron.* **72**, 1079
- [33] Bogdashov AA et al 2005, *Int. J. Infrared and Millimeter Waves* **26**, 771
- [34] Thumm M et al 2007, *IEEE Trans. on Plasma Science* **35**, 143
- [35] Neilson JF 2006, *IEEE Trans. on Plasma Science* **34**, 635
- [36] Chirkov AV et al 2006, *Radiophys. Quantum Electron.* **49**, 344
- [37] Jin J, et al 2009, *IEEE Trans. on Microwave Theory and Techniques* **57**, 1661
- [38] Neilson JF and Bunker R 2002 *IEEE Trans. on Plasma Science* **30**, 794
- [39] Jin J et al 2017, *IEEE Trans. on Microwave Theory and Techniques* **65**, 3, 699
- [40] Thumm M 1998, *Int. J. Infrared and Millimeter Waves* **19**, 3
- [41] Braz O et al 1997, *Int. J. Infrared and Millimeter Waves* **18**, 1495
- [42] Kasugai A et al 1998, *Rev. Sci. Instruments* **69**, 2160
- [43] Sakamoto K et al 1999, *Rev. Sci. Instruments* **70**, 208.
- [44] Sakamoto K et al 1994, *Phys. Rev. Lett.* **73**, 3532
- [45] Piosczyk B et al 1996, *IEEE Trans. on Plasma Science* **24**, 579
- [46] Denisov G et al 2017, *EPJ Web of Conferences* **147**, 04003
- [47] Schmid M, Illy S, Dammertz G, Erckmann V and Thumm M 2007 *Fusion Eng. Design* **82**, 744
- [48] Thumm M et al. 2008, *IEEE Trans. on Plasma Science* **36**, 341
- [49] Ives RL et al 1999, *IEEE Trans. on Plasma Science* **27**, 2, 531
- [50] Bruschi et al 2003, *Nucl. Fusion* **43**, 1513
- [51] Schlaich A et al 2013, *IEEE Trans. on Microw. Theory and Techniques* **61**, 4660
- [52] Chirkov AV, Denisov GG and Aleksandrov NL 1995 *Opt. Commun.* **115**, 449
- [53] Darbos C et al 2015, *J. Infrared, Millimeter, and Terahertz Waves* **37**, 4
- [54] Bigot B 2018, *27th IAEA Int. Conf. on Fusion Energy (Gandhinagar, India, 2018)* [OV/1-2]
- [55] Sakamoto K. et al 1996, *J. Phys. Soc. Japan* **65**, 1888.
- [56] Sakamoto K. et al 1997, *Int. J. Infrared and Millimeter Waves* **18**, 1637.
- [57] Sakamoto K et al 2007, *Nature Physics* **3**, 411
- [58] Kasugai A et al 2008, *Nucl. Fusion* **48**, 054009
- [59] Sakamoto K et al 2009, *Nucl. Fusion* **49**, 095019
- [60] Kajiwara K et al 2013, *Nucl. Fusion* **53**, 043013
- [61] Kajiwara K et al 2011, *J. Infrared, Millimeter and Terahertz Waves* **32**, 329
- [62] Kajiwara K et al 2011, *Fusion Eng. and Design* **86**, 955
- [63] Ikeda R et al 2015, *Fusion Eng. and Design* **96-97**, 482
- [64] Oda Y et al 2018, *27th IAEA Int. Conf. on Fusion Energy (Gandhinagar, India, 2018)* [FIP/P1-56]
- [65] Zapevalov VE et al 2001, *Fusion Eng. and Design* **53**, 377
- [66] Denisov GG et al 2003, *Radiophysics and Quantum Electronics* **46**, 757
- [67] Denisov GG et al 2008, *Nucl. Fusion* **48**, 054007
- [68] Litvak AG et al 2011, *J. Infrared, Millimeter and Terahertz Waves* **32**, 337
- [69] Krasilnikov AV et al 2015, *Nucl. Fusion* **55**, 10, 104007
- [70] *ITER Newslines*, 26 February 2018, <https://www.iter.org/newsline/-/2931>
- [71] Darbos C et al 2019, *J. Infrared, Millimeter and Terahertz Waves*, in press
- [72] Hogge J-P et al 2009, *Fusion Science and Technology* **55**, 204
- [73] Pagonakis IGr et al 2015, *Fusion Eng. and Design* **96-97**, 149
- [74] Rzesnicki T et al 2017, *Fusion Eng. and Design* **123**, 490
- [75] Gantenbein G et al 2017, *EPJ Web of Conferences* **157**, 03016
- [76] Ioannidis ZC et al 2017, *IEEE Trans. on Electron Devices* **64**, 9, 3885
- [77] Imai T et al 2010, *23rd IAEA Int. Conf. on Fusion Energy (Daejeon, South Korea, 2010)* TP/P6-12
- [78] Minami R et al 2013, *Nucl. Fusion* **53**, 063003
- [79] Kariya T et al 2017, *Nucl. Fusion* **57**, 066001
- [80] Kariya T et al 2018, *27th IAEA Int. Conf. on Fusion Energy (Gandhinagar, India)* [FIP/P1-56]
- [81] Moriyama S et al 2009, *Nucl. Fusion* **49**, 085001
- [82] Kobayashi T et al 2015, *Nucl. Fusion* **55**, 063008
- [83] Denisov GG et al 2017, *18th IEEE Int. Vacuum Electron. Conf. (IVEC 2017)*, London, UK, GI-1
- [84] Erckmann V et al 2007, *Fusion Science and Technology* **52**, 291
- [85] Felch K et al 2005, *J. of Physics: Conference Series* **25**, 13
- [86] Cauffman et al 2015, *40th Int. Conf. Infrared, Millimeter and Terahertz Waves*, Hong Kong, M1E5
- [87] Alberti S et al 2001, *Fusion Eng. and Design* **53**, 387

- 1
2
3 [88] Dammertz G et al 2002, *IEEE Trans. on Plasma Science* **30**, 808
4 [89] Dammertz G et al 2005, *Fusion Eng. and Design* **74**, 217
5 [90] Gantenbein G et al 2011, *J. of Infrared, Millimeter, and Terahertz Waves*, **32**, 320
6 [91] Thumm M et al 2005, *IEEE Trans. on Electron Devices* **52**, 818
7 [92] Dammertz G et al 2003, *Fusion Eng. and Design* **66-68**, 497
8 [93] Darbos C et al 2009, *Fusion Science and Technology* **56**, 1205
9 [94] Wagner D. et al 2015, *J. Infrared, Millimeter and Terahertz Waves* **37**, 1, 45
10 [95] Alberti S et al 2017, *EPJ Web of Conferences* **157**, 03001
11 [96] Rodolphe M et al 2019, *20th Int. Conf. Vacuum Electronics (IVEC 2019)*, Busan, South Korea
12 [97] Felch K, Huey H, and Jory H 1990, *J. Fusion Energy* **9**, 59
13 [98] Felch K et al 1996, *IEEE Trans. on Plasma Science* **24**, 558
14 [99] Felch K et al 2008, *Nucl. Fusion* **48**, 054008
15 [100] Lohr J et al 2011, *J. Infrared, Millimeter and Terahertz Waves* **32**, 253
16 [101] Choi EM et al 2006, *Phys. Plasmas* **13**, 023103
17 [102] Felch K et al 2015, *EPJ Web of Conferences* **87**, 04006
18 [103] Felch K et al 2017, *42nd Int. Conf. Infrared, Millimeter, and THz Waves*, Cancun, Mexico, WC2.3
19 [104] Zohm H and Thumm M 2005, *J. Phys.: Conf. Ser.* **25**, 274
20 [105] Piosczyk B et al 2000, *IEEE Trans. on Plasma Science* **28**, 918
21 [106] Zapevalov VE et al 2004, *Radiophysics and Quantum Electronics* **47**, 396
22 [107] Kazansky IV et al 2009, *7th Int. Workshop Strong Microwaves: Sources and Applications* **1**, 100
23 [108] Sakamoto K et al 2017, *42nd Int. Conf. Infrared, Millimeter, and THz Waves*, Cancun, Mexico,
24 RA2.3
25 [109] Morozkin M et al 2018, *EPJ Web of Conferences* **195**, 01008
26 [110] Denisov GG et al 2018, *Review of Scientific Instruments* **89**, 084702
27 [111] Garavaglia S et al 2018, *Fusion Eng. and Design* **136**, 1173
28 [112] Franck J et al 2015, *Nucl. Fusion* **55**, 013005
29 [113] Thumm M et al 2015, *Terahertz Science and Technology* **8**, 3, 85
30 [114] Kalaria PC et al 2016, *Phys. Plasmas* **23**, 092503
31 [115] Kalaria PC et al 2017, *Frequenz* **71**, 3-4, 161
32 [116] Jelonnek J et al 2017, *Fusion Eng. and Design* **123**, 241
33 [117] Thumm M et al 2018, *Terahertz Science and Technology* **11**, 1, 1
34 [118] Ruess T et al 2019, *20th Int. Conf. Vacuum Electronics (IVEC 2019)*, Busan, South Korea
35 [119] Schmid M et al 2017, *Fusion Eng. and Design* **136**, 485
36 [120] Saito T et al 2012, *Phys. Rev. Lett.* **109**, 15, 155001
37 [121] Saito T et al 2013, *38th Int. Conf. Infrared, Millimeter, and THz Waves*, Mainz, Germany, Mo5-3
38 [122] Saito T et al 2017, *Plasma and Fusion Res.: Rapid Communications* **12**, 1206013
39 [123] Glyavin MY et al 2012, *Appl. Phys. Lett.* **101**, 15, 153503
40 [124] Fokin A et al 2018, *Scientific Reports* **8**, 4317
41 [125] Kajiwara K et al 2011, *Appl. Phys. Express* **4**, 126001
42 [126] Sakamoto K et al 2012, *37th Int. Conf. Infrared, Millimeter, and THz Waves*, Wollongong,
43 Australia, Tue-A-3-1
44 [127] Ikeda R et al 2017, *J Infrared Millimeter and Terahertz Waves* **38**, 531
45 [128] Oda Y et al 2018, *Nucl. Fusion* **58**, 106041
46 [129] Braz O et al 1997, *Int. J. Infrared and Millimeter Waves* **18**, 1465
47 [130] Thumm M et al 2001, *Fusion Eng. and Design* **53**, 407
48 [131] Hirose R et al 2008, *IEEE Trans. Applied Superconductivity* **18**, 2, 920
49 [132] Litvak AG et al 2012, *EPJ Web of Conferences* **32**, 04003
50 [133] Koppenburg K et al 2001, *IEEE Trans. on Electron Devices* **48**, 101
51 [134] Gantenbein G et al 2014, *IEEE Trans. on Electron Devices* **61**, 6, 1806
52 [135] Samartsev A et al 2015, *IEEE Trans. on Electron Devices* **62**, 7, 2317
53 [136] Piosczyk B et al 2004, *IEEE Trans. on Plasma Science* **32**, 853
54 [137] Zapevalov VE et al 2000, *Radiophysics and Quantum Electronics* **43**, 671
55 [138] Piosczyk B et al 1997, *IEEE Trans. on Plasma Science* **25**, 460
56 [139] Rzesnicki T et al 2010, *IEEE Trans. on Plasma Science* **38**, 1141
57 [140] Ruess S et al 2018, *Int. J. Microwave and Wireless Technologies* **10**, 547
58 [141] Gantenbein G et al 2019, *Fusion Eng. and Design*, doi.org/10.1016/j.fusengdes.2018.12.063
59
60

- 1
2
3 [142] Flyagin VA et al 2003, *Int. J. Infrared and Millimeter Waves* **24**, 1
4 [143] Ioannidis ZC et al 2016, *IEEE Trans. on Electron Devices* **63**, 3, 1299
5 [144] Chirkov AV, Denisov GG and Kuftin AN 2015, *Applied Physics Letters* **106**, 263501
6 [145] Denisov GG 2017, *EPJ Web of Conferences* **149**, 01001
7 [146] Bakunin VL et al 2018, *Technical Physics Letters* **44**, 6, 473
8 [147] Faillon G et al 2008, “Microwave Tubes”, “*Vacuum Electronics – Components and Devices*”,
9 Eichmeier JA and Thumm M, eds., Springer, Berlin Heidelberg New York, 1-84 (2008)
10 [148] Ives RL et al 1999, *IEEE Trans. on Plasma Science* **27**, 503
11 [149] Pagonakis IGr et al 2008, *IEEE Trans. on Plasma Science* **36**, 469
12 [150] Wu C et al 2018, *Phys. Plasmas* **25**, 033108
13 [151] Wu C et al 2019, *Phys. Plasmas* **26**, 013108
14 [152] Wilde F et al 2017, *18th IEEE Int. Vacuum Electron. Conf. (IVEC 2017)*, London, UK, GII-1
15 [153] Wilde F et al 2018, *20th Joint Workshop on ECE and ECRH (EC20)*, Greifswald, Germany, S4.4.
16 [154] Wagner D et al 2017, *EPJ Web of Conferences* **149**, 03004
17 [155] Cengher M et al 2019, *EPJ Web of Conferences* **203**, 02006
18 [156] Wang X et al 2019, *EPJ Web of Conferences* **203**, 02012
19 [157] Park HK et al 2018, *27th IAEA Int. Conf. on Fusion Energy (Gandhinagar, India)* [OV/2-3]
20 [158] Coda S et al 2018, *27th IAEA Int. Conf. on Fusion Energy (Gandhinagar, India)* [OV/5-2]
21 [159] Borschegovskiy A et al 2019, *EPJ Web of Conferences* **203**, 02004
22 [160] Igami, H et al 2019, *EPJ Web of Conferences* **203**, 02001
23
24
25
26
27
28
29
30
31
32
33
34
35
36
37
38
39
40
41
42
43
44
45
46
47
48
49
50
51
52
53
54
55
56
57
58
59
60